



Walowski, K. J., Kirstein, L. A., De Hoog, J. C. M., Elliott, T. R., Savov, I. P., Jones, R. E., & University of Edinburgh (2019). Investigating ocean island mantle source heterogeneity with boron isotopes in melt inclusions. *Earth and Planetary Science Letters*, 508, 97-108.  
<https://doi.org/10.1016/j.epsl.2018.12.005>

Peer reviewed version

License (if available):  
CC BY-NC-ND

Link to published version (if available):  
[10.1016/j.epsl.2018.12.005](https://doi.org/10.1016/j.epsl.2018.12.005)

[Link to publication record in Explore Bristol Research](#)  
PDF-document

This is the author accepted manuscript (AAM). The final published version (version of record) is available online via Elsevier at <https://www.sciencedirect.com/science/article/pii/S0012821X18307143?via%3Dihub> . Please refer to any applicable terms of use of the publisher.

## University of Bristol - Explore Bristol Research

### General rights

This document is made available in accordance with publisher policies. Please cite only the published version using the reference above. Full terms of use are available:  
<http://www.bristol.ac.uk/red/research-policy/pure/user-guides/ebr-terms/>

**Investigating ocean island mantle source heterogeneity with boron isotopes in melt inclusions**

Walowski, K.J.<sup>1, 2\*</sup>, Kirstein, L.A.<sup>1</sup>, De Hoog, J.C.M.<sup>1</sup>, Elliot, T.<sup>3</sup>, Savov, I.P.<sup>4</sup>, Jones, R.E.<sup>5</sup>, EIMF<sup>6</sup>

<sup>1</sup> University of Edinburgh, School of Geosciences, Grant Institute, Edinburgh, UK

<sup>2</sup> Middlebury College, Department of Geology, Middlebury, VT, USA

<sup>3</sup> University of Bristol, School of Earth Sciences, Bristol, UK

<sup>4</sup> University of Leeds, School of Earth and Environment, Leeds, UK

<sup>5</sup> University of Oxford, Department of Earth Sciences, Oxford, UK

<sup>6</sup> Edinburgh Ion Microprobe Facility, Grant Institute, University of Edinburgh, Edinburgh, UK

\*Corresponding Author - Current contact information: kwalowski@middlebury.edu

Keywords: Ocean island basalts; Mantle Volatiles; Mantle Geochemistry; Boron Isotopes; Melt inclusions; Geochemistry; Volatile Recycling

**Abstract**

Recycling of the lithosphere via subduction drives the trace element and isotopic heterogeneity of the mantle, yet, the inventory of volatile elements in the diverse array of mantle reservoirs sampled at ocean islands remains uncertain. Boron is an ideal tracer of

volatile recycling because it behaves similarly to volatiles during high-temperature geochemical reactions and carries a distinctive isotope signature into the mantle, but is subsequently little-influenced by degassing on return to the surface. Furthermore, B-rich recycled lithologies will have a strong influence on typical upper mantle compositions characterized by low B concentrations ( $<0.2 \mu\text{g/g}$  and  $\delta^{11}\text{B} -7.1\pm0.9\text{‰}$ ). Here, we present and compare the B abundances and isotope compositions, together with the volatile element contents ( $\text{H}_2\text{O}$ ,  $\text{CO}_2$ , and Cl) of basaltic glasses and olivine-hosted melt inclusions from two different ocean island localities (La Palma, Canary Islands, and Piton de Caille, La Réunion Island). Our results suggest that olivine hosted melt inclusions are protected from contamination during ascent and provide more robust estimates of primary mantle source  $\delta^{11}\text{B}$  than previous bulk rock studies. We find that the  $\delta^{11}\text{B}$  of the La Réunion samples ( $-7.9\pm0.5\text{‰}$  ( $2\sigma$ )) overlaps with the recently defined MORB datum, indicating that the depleted upper-mantle and ‘primitive mantle’ reservoirs are indistinguishable with respect to  $\delta^{11}\text{B}$ , or that B concentrations are sufficiently low that they are diluted by partial melting in the uppermost mantle. In contrast, the La Palma samples, notable for their radiogenic Pb isotope ratios, are characterized by  $\delta^{11}\text{B}$  values that are distinctly isotopically lighter ( $-10.5\pm0.7\text{‰}$  ( $2\sigma$ )) than La Réunion or MORB. We suggest these isotopically light values are derived from significantly dehydrated recycled materials preserved in the La Palma mantle source region, in keeping with their lower B/Zr and  $\text{H}_2\text{O}/\text{Ce}$ . This work therefore provides strong new support for subduction zone processing as a mechanism for generating radiogenic Pb isotopic signatures and volatiles heterogeneities in the mantle.

## 1. Introduction

Physical and chemical interactions between the mantle and the Earth's surface have controlled the long-term evolution of the crust, the oceans, and the atmosphere. The mantle is a potentially major reservoir of the volatile elements, which in turn can have a major effect on the physical properties the Earth's interior (e.g., Jung and Karato, 2001). Yet, the volatile element composition of the Earth's interior remains poorly characterized. Tectonic recycling of oceanic lithosphere, specifically, is a key control of the volatile element distribution in the Earth's interior and is also thought to have generated mantle heterogeneity throughout Earth's history for a range of other elements (e.g. Allègre 1982, Hofmann and White, 1982). Indeed, our understanding of the influence of subducted recycled material on mantle composition, reflected in compositional variability in ocean island basalts (OIB) and to a lesser extent mid-ocean ridge basalt (MORB), remains largely supported by the initial observations made in the early 1980s based on the modest selection of isotope systems (Sr, Nd, Pb) that could be measured with sufficient precision at the time (e.g., Zindler and Hart, 1986). Subsequent work utilizing other stable isotope systems such as O, Fe, Li, Mg, U, Tl and Cl isotopes have provided continued support for recycling of surficial materials into the deep mantle (e.g., Eiler et al., 1997; Turner et al., 1997; Ryan and Kyle, 2004; Teng et al., 2010, Nielson et al., 2006; Williams and Bizimis, 2014) but, the origin of various indices of source heterogeneity continue to be debated.

An important step forward would be to link mantle heterogeneities with volatile elements that intrinsically represent a distinct part of the recycling process. However, the volatile character and composition of different mantle end-members remains poorly



understood. Recent work from Dixon et al. (2017) utilizing enriched MORB compositions provides initial evidence that volatiles and their light stable isotopes, primarily  $\delta D$ , may become decoupled from other lithophile elements through a complex multistage dehydration and re-equilibration journey of subducting slabs from the surface to the transition zone.

A perfect tracer for slab recycling should be only fractionated at the Earth's surface, have a strong influence on mantle compositions but be resistant to perturbations en route back to the surface, all of which apply to B (De Hoog and Savov, 2018). Boron is strongly enriched and isotopically fractionated in altered oceanic crust (e.g., Smith et al., 1995; Nakamura et al., 1992), serpentinized oceanic lithospheric mantle (e.g., Pabst et al., 2012; Harvey et al., 2014), and sediments (e.g., Ishikawa and Nakamura, 1993; Tonarini et al., 2011; *for a detailed data compilation see* Marschall, 2018 and references therein). The mantle is strongly depleted in B due to its relatively incompatible nature (similar to LREE; Ryan et al., 1996; Ishikawa & Tera, 1999; Marschall et al., 2017) and so, recycled slab materials, where and if present, should have a significant impact on mantle B abundances and their isotopic makeup (Marschall et al., 2018). Thus, B isotopes have the potential to track the fate of recycled lithosphere, which may also be a major repository of water, halogens and noble gases in the deep mantle (Kendrick et al., 2012).

A number of studies have employed boron concentrations and isotope ratios in an attempt to characterize recycled components in OIB mantle sources (e.g., Ryan et al., 1996; Chaussidon and Marty, 1995; Gurenko and Chaussidon, 1997). However, the data interpretation of these previous studies suffered from a poorly-defined baseline for

MORB and DMM, and inclusion of samples that had assimilated hydrothermally altered materials (see Marschall et al., 2017), or inadequate analytical precision. In this study, we build upon recent improvements to the in-situ analytical techniques for measuring  $\delta^{11}\text{B}$  in low boron concentration samples (e.g., Marschall and Monteleone, 2015), including the improved characterization of glassy reference materials (e.g., Rosner and Meixner, 2004) and contrast new measurements against a comprehensive reassessment of the  $\delta^{11}\text{B}$  variability within a global MORB dataset (Marschall et al., 2017).

To test the capabilities of B isotopes as a tracer for recycled oceanic crust, here, we compare contrasting OIBs from La Réunion Island with high  $\text{He}^3/\text{He}^4$  (Hanan & Graham, 1996), elevated  $^{207}\text{Pb}/^{204}\text{Pb}$  and old model ages (Chase, 1981), possibly Hadean (Peters et al., 2018), to those from La Palma which display radiogenic Pb and trend toward the so-called HIMU end-member (“high  $\mu$ ” where  $\mu = ^{238}\text{U}/^{204}\text{Pb}$ ; Zindler and Hart, 1986). The mantle source of the La Réunion magmas thus represents a ‘primitive mantle’ composition, potentially little modified over Earth’s history (comparable to the ‘primitive helium mantle’ or ‘the common mantle component;’ Farley et al., 1992 and Hanan and Graham, 1996, respectively). Conversely, the HIMU end-member, characterized by elevated  $^{206}\text{Pb}/^{204}\text{Pb}$  ratios at low  $^{87}\text{Sr}/^{86}\text{Sr}$  ratios, is consistently suggested to be formed, in part, by recycled ancient subduction-modified crust (Fig. 1; Chauvel et al., 1992; Marcantonio et al., 1996; Day et al., 2010). A key aspect of this study is that we have analyzed melt inclusions. The necessity for this is two-fold: (1) olivine host-phenocrysts can shield the sample from crustal and seawater contamination/assimilation which may overprint the  $\delta^{11}\text{B}$  of the mantle source (Rosner et al., 2004; 2008; Gurenko & Kamenetsky, 2011), and (2) melt inclusions provide the best

estimates of initial volatile concentrations which can be utilized to infer mantle source volatile concentrations (e.g., Michael et al., 1995) as well as minimum estimates of crystallization depths (e.g., Newman and Lowenstern, 2000). Despite the potential for various post-entrapment modification processes in melt inclusions (Wallace et al., 2015 and references there within), our study focuses on the most valuable, rapidly quenched samples (i.e. loose olivine from the coarse-ash sized fraction of a tephra deposit, as opposed to olivine phenocrysts found within a thick, slowly cooled lava flow or larger scoria clasts/bombs; e.g., Lloyd et al., 2013) and employs well-established post-entrapment crystallization corrections (e.g., Danyushevsky et al., 2002; Lloyd et al., 2013; Wallace et al., 2015) to determine the best estimates of pre-eruptive volatiles possible.

Hence, we aim to re-examine how two different deep mantle sources compare in their  $\delta^{11}\text{B}$  system to MORB, and determine the volatile ( $\text{H}_2\text{O}$ ,  $\text{CO}_2$ , Cl, and F) composition of basaltic melt inclusions to better understand the concentrations and distribution of volatiles in deep recycled mantle material.

## **2. Sample Locations and Descriptions**

### **2.1 Piton de Caille, Piton de la Fournaise, Réunion Island**

Piton de la Fournaise is one of the most active hotspot volcanoes on Earth, and represents the most recent expression of a long-lived mantle plume which previously formed the Deccan Traps (65 Ma; Albarède, 1997 and reference there within). The island is situated on oceanic crust that is ~64 Ma, and typically erupts transitional aphyric

basalts and picritic basalts along fissures, although more explosive Strombolian activity also produces fire-fountaining and builds scoria cones. Piton de Caille represents one such scoria cone found in the NW rift zone that erupted <5000 years ago (Bureau et al., 1998). In this study, we have acquired samples of wind-sorted olivine-rich material derived from the Piton de Caille vent. The olivine phenocrysts from this sample are large (1-5mm) and contain numerous large glassy melt inclusions.

Primitive magmas erupted from Piton de la Fournaise are generally characterized by tholeiitic compositions (e.g., Albarède, 1997) and are thought to be derived from mantle with elevated potential temperatures indicative of a deep-seated plume source (e.g., Sobolev and Nikogosian, 1994). In addition, a restricted range of  $^{187}\text{Os}/^{188}\text{Os}$  ratios indicate a relatively homogenous source that has not been significantly affected by oceanic crust and/or continental sediment inputs (Schiano et al., 2012), while high  $^3\text{He}/^4\text{He}$  and  $^{142}\text{Nd}$  indicate this reservoir has potentially been isolated from significant mantle mixing since the Hadean (Peters et al., 2018). These numerous characteristics provides a basis for the sample choice as an example of an OIB that represents melting of relatively undisturbed and deeply sourced primitive mantle.

## **2.1 La Palma, The Canary Archipelago**

The Canary Archipelago, located offshore NW Africa, is a westward-younging volcanic island chain suggested to be the result of a low buoyancy or weak mantle plume impinging beneath the African plate (Schminke, 1982). La Palma is one of the most recently active island in the Canaries, still in its shield building phase and is built on oceanic crust ~160 Ma in age. Magmas erupted at La Palma are highly silica-

undersaturated, befitting its position atop thick lithosphere (e.g., McBirney and Gass, 1967). La Palma lavas have radiogenic Pb isotopic compositions but relatively unradiogenic Sr isotope ratios (Fig. 1), a so-called HIMU affinity, which has been widely interpreted to reflect the contribution of recycled mafic crust (Zindler and Hart 1986). This general inference has been further supported by highly radiogenic Os isotope ratios (Marcantonio et al., 1996) and low  $\delta^{18}\text{O}$  (Day et al., 2010). Evidence for a recycled component in the La Palma mantle source and access to appropriate samples thus provides a contrast to the La Réunion samples to test the effectiveness of boron isotopes in tracking recycled material in OIB mantle sources.

La Palma additionally provides a wealth of young, explosive cone deposits from which to collect samples for melt inclusion work. The island is comprised of two main edifices, the extinct ~1 Ma Taburiente Shield in the north, and the historically active Cumbre Vieja Ridge (Hernandez-Pacheco and Valls, 1982). Samples for this study were acquired from both edifices. From Taburiente, two scoria samples were collected from a relict cone interbedded in a ~0.7 Ma continuous lava sequence exposed in the Barranco Fagundo (Fig. 2; Supplementary Table TS1), the locality from which previous studies measured the highest Pb isotope ratios (Nikogosian et al., 2002). From the Cumbre Vieja Ridge, coarse-ash was sampled from a road-cut Holocene-age cone at the northernmost extension of the Cumbre Vieja Ridge, and from the 1949 eruption of Vólcan Duraznero (Fig. 2; Supplementary Table TS1). A detailed description of sample localities is provided in Supplementary Table TS1.

### **3. Methods**

### 3.1 Sample preparation and analytical methods

All samples analyzed in this study are derived from the coarse-ash size fraction of tephra deposits. This type of material was collected to obtain naturally quenched inclusions in order to minimize the potential for syn-eruptive diffusive loss of volatile elements (e.g., hydrogen; Lloyd et al., 2013) or crystallization of melt inclusions. Individual loose olivine phenocrysts (250  $\mu\text{m}$  to 2 mm in length) were hand-picked from sieved tephra and examined in immersion oils or alcohol to locate the melt inclusions. Olivine crystals hosting fully enclosed, glassy melt inclusions were mounted in acetone-soluble acrylic resin in 5mm diameter aluminum rounds and individually polished to expose melt inclusions. Polished olivine phenocrysts hosting melt inclusions were then removed from the acrylic resin following a 3-step treatment in acetone and subsequently remounted in epoxy resin mounts. The final epoxy mounts were polished, cleaned and coated in Au.

The samples were first analyzed for boron isotope ratios ( $\delta^{11}\text{B}$ ) using the Cameca IMS-1270 secondary ion mass spectrometer at the NERC Edinburgh Ion Microprobe Facility (EIMF). The uncertainties of the measurements were typically ca. 1.0‰ (1s) for B concentrations of 1-3 ppm, whereas the accuracy is estimated as 0.9‰ based on the average deviation of calibration standards from their reference values (see Supplementary Materials, Section 1. Analytical Methodology, for details). Following B-isotope analyses, volatile ( $\text{H}_2\text{O}$ ,  $\text{CO}_2$ , Cl, and F) and selected trace elements (Rb, Sr, Y, Zr, Nb, Ba, La, and Ce) were analyzed in the same melt inclusions using a Cameca IMS-4f SIMS at EIMF using separate analytical routines for  $\text{CO}_2$  and all remaining elements. Lastly, melt inclusions and host olivine were analyzed for major elements on the Cameca SX-100

electron microprobe at the University of Edinburgh. A complete description of all analytical methods is provided in the Supplementary Materials (Section 1. Analytical Methodology), while additional details of calibrations and reproducibility of  $\delta^{11}\text{B}$  analyses can be found in Supplementary Table TS4 and TS5.

### **3.2 Melt inclusion corrections**

Samples used in this study provided olivine phenocrysts hosting fully-enclosed glassy melt inclusions. However, it is well-known that even the most pristine melt inclusions may have been modified after entrapment (e.g., Esposito et al., 2011; Gaetani et al., 2012). Melt inclusions are typically affected by crystallization of olivine along the walls of the inclusion and by Fe diffusive loss during the time between trapping and eruption (post-entrapment crystallization; PEC; Danyushevsky et al., 2000). The major element compositions of the inclusions were corrected for this PEC and Fe-loss using Petrolog 3.1.1.3 (Danyushevsky and Plechov, 2011), using models for olivine-melt equilibria from Putirka et al. (2005) and oxidation state from Borisov and Shapkin (1990). Concentrations of volatiles and trace elements that are incompatible in the olivine hosts were corrected using the Petrolog results for the major elements. Initial Fe-contents were chosen based on the highest value of  $\text{FeO}^{\text{T}}$  for a melt inclusion suite from each sample. An average oxygen fugacity of  $\Delta\text{QFM}+0.6$  was used in the Petrolog calculations based on previous average estimates of  $f\text{O}_2$  from La Réunion (Brounce et al., 2017).

## **4. Results**

### **4.1 Major element compositions**

#### 231 4.1.1 Piton de Caille, La Réunion

232 From the Piton de Caille sample, 23 olivine phenocrysts hosting glassy melt  
233 inclusions were successfully prepared and analyzed. The olivine host crystals vary from  
234 Fo<sub>81</sub> to Fo<sub>86</sub> (Table 1). Corrected melt inclusions (see section 3.2) are basaltic and  
235 subalkaline in composition (Supplementary Fig. 1), consistent with previous studies of  
236 samples from the same localities (Bureau et al., 1998). The corrected MgO contents range  
237 from ~7-11 wt% (Fig. 4; Table 1), and show little correlation with other major elements  
238 (i.e., Al<sub>2</sub>O<sub>3</sub>, Fig. 4) suggesting only minor olivine and clinopyroxene (CPX) fractionation  
239 has affected the lowest-MgO melt inclusions. These observations suggest that the  
240 analyzed melt inclusions represent relatively primitive mantle melts, and should provide  
241 an adequate representation of their mantle source compositions.

#### 243 4.1.2 La Palma Suite

244 From the La Palma samples, 44 olivine phenocrysts hosting glassy melt inclusions  
245 and 3 subaerial glass beads were successfully prepared and analyzed. Of these, 10 melt  
246 inclusions and the glass beads were derived from Barranco Fagundo 01 (BF01), 4 melt  
247 inclusions from Barranco Fagundo 02 (BF02), 9 from the Holocene cone, and 21 from  
248 the 1949 eruption of Vólcan Duraznero (Fig. 1).

249 The sample BF01 contains olivine phenocrysts Fo<sub>82</sub> to Fo<sub>86</sub> in composition, while  
250 BF02 contains distinctly less primitive olivine phenocrysts, Fo<sub>76</sub> to Fo<sub>79</sub> in composition  
251 (Table 1). Corrected melt inclusions from both samples are alkaline basalts, although  
252 those from BF01 are more primitive than those from BF02, containing MgO contents of  
253 ~10 wt%, compared with ~6 wt% (Table 1; Fig. 3). We also analyzed glass bead samples



from BF01 (i.e. glass not contained within olivine crystals) which represent melts that have fractionated relative to associated melt inclusions compositions (Fig. 3). The Holocene cone sample contains olivine phenocrysts ranging in composition from Fo<sub>79</sub> to Fo<sub>85</sub>. Corrected melt inclusions are basanitic in composition and display a large range in MgO contents from ~6-10 wt%. Melt inclusions from the 1949 eruption of Vólcan Duraznero are hosted in olivine phenocrysts ranging in composition from Fo<sub>79</sub> to Fo<sub>84</sub>. Corrected melt inclusions are basanitic in composition and display a range in MgO contents from ~6-10 wt%.

Comparing the La Palma samples, we find a negative correlation between MgO and Al<sub>2</sub>O<sub>3</sub>, which indicates that variability between samples is dominantly the result of CPX and olivine fractionation. The sample BF01 is the most primitive sample, overlapping in composition with the most primary La Palma magmas, as defined by Day et al. (2010). The major element composition of the remainder of the samples have been variably influenced by fractionation of both CPX and olivine.

## **4.2 Volatile and halogen compositions**

### *4.2.1 Piton de Caille, Réunion*

Dissolved H<sub>2</sub>O and CO<sub>2</sub> contents of the Piton de Calle melt inclusions, after correction for PEC and Fe-loss, range between 0.87-1.08 wt% and 949-1468 µg/g, respectively. The Cl compositions are also corrected for PEC and range from 172-432 µg/g. As shown in Figure 3c, melt inclusions compositions cluster along an open system degassing path calculated using the Sol\_Ex software (Witham et al., 2012) assuming initial volatile contents represented by the composition of the highest measured H<sub>2</sub>O and

CO<sub>2</sub> (1.08 wt% and 14681 µg/g, respectively). A lack of significant variability in H<sub>2</sub>O contents suggests that individual melt inclusions suffered little post-entrapment hydrogen loss (Lloyd et al., 2013; Bucholz et al., 2013). Rather, most variability can be explained by differences in the extent of pre-entrapment degassing (e.g., Johnson et al., 2009) and/or post-entrapment loss in CO<sub>2</sub> (e.g., Wallace et al., 2015; Moore et al., 2015). Although it is difficult to determine which of these two processes controls the observed variability in CO<sub>2</sub>, it is important to note most melt inclusions analyzed in this study contain a vapor bubble and such bubbles typically contain a substantial fraction (40-90%) of the CO<sub>2</sub> that was initially dissolved in the trapped melt (Wallace et al., 2015; Moore et al., 2015). As such, the CO<sub>2</sub> contents of the melt inclusions are likely underestimates of the original magmatic CO<sub>2</sub> content. Therefore, estimated depths of entrapment calculated using the Sol-Ex software (Witham et al., 2012) represent minimum estimates of crystallization depths of ~7.5 km.

Corrected volatile compositions are compared to published data from Piton de Caille (Bureau et al., 1998) and other vents associated with Piton de la Fournaise (Vigouroux et al., 2009). These comparisons show that the Piton de Caille melt inclusions retain higher volatile contents than those from other La Reunion vents (Fig. 3c).

#### *4.2.2 La Palma, Canary Islands*

Dissolved H<sub>2</sub>O and CO<sub>2</sub> contents of La Palma melt inclusions, after correction for PEC and Fe-loss, range between 0.03-1.96 wt% and 0-4303 µg/g, respectively. The Cl compositions are also corrected for PEC and range from 656-1633 µg/g. All samples show greater amounts of scatter than observed in data from Piton de Caille. As shown in

Figure 3d, melt inclusions compositions scatter around an open-system degassing path calculated using the Sol\_Ex software (Witham et al., 2012) assuming initial volatile contents represented by the composition of the highest measured H<sub>2</sub>O and CO<sub>2</sub> melt inclusions from BF01 (1.52 wt% and 4072 µg/g, respectively).

Interestingly, data from Vólcan Duraznero appear to show two different open-system degassing paths (one of which originates at ~0.4 wt% H<sub>2</sub>O), which may indicate mixing of two magmas stored at different depths. The presence of multiple magma batches is consistent with observations described in Klügel et al., (2005), but here we simply focus on the H<sub>2</sub>O-rich population as the best minimum estimate of the pre-eruptive H<sub>2</sub>O contents.

#### *4.4 Boron concentrations and $\delta^{11}\text{B}$*

Boron concentrations of corrected melt inclusions from Réunion have an average of  $2.46 \pm 0.31$  µg/g, while La Palma magmas have concentrations between 1.8-4.7 µg/g (Fig 4a). These values are consistent with previous bulk rock measurements of high-MgO OIB (Ryan et al., 1996).

The average  $\delta^{11}\text{B}$  of melt inclusions from Réunion is  $-7.9 \pm 0.5\text{‰}$  ( $2\sigma$ ), which overlap within uncertainty of the newly established global MORB value ( $-7.1 \pm 0.9\text{‰}$  Marschall et al., 2017). At La Palma, melt inclusions have  $\delta^{11}\text{B}$  that extend to lighter values. The melt inclusions from BF01 have the lightest average,  $-10.5 \pm 0.7\text{‰}$ , while BF02 melt inclusions have an average  $\delta^{11}\text{B}$  of  $-8.2 \pm 0.7\text{‰}$  and BF01 glass beads have an average of  $-8.4 \pm 0.6\text{‰}$ . The Holocene cone and Vólcan Duraznero have averages of  $-9.9 \pm 1.1\text{‰}$ , and  $-10 \pm 0.7\text{‰}$ , respectively.

323 As shown in Figure 4,  $\delta^{11}\text{B}$  values do not correlate with B concentrations.  
324 Additionally, the  $\delta^{11}\text{B}$  values do not display convincing correlations between other major  
325 elements or trace element ratios, such as La/Nb. Thus, observed within-sample variation  
326 in  $\delta^{11}\text{B}$  is likely the result of analytical uncertainty, as opposed to magmatic processes  
327 such as fractionation or partial melting, as previously suggested for the B isotope system.

328 Overall,  $\delta^{11}\text{B}$  values from La Palma and La Réunion samples in this study overlap  
329 with those previously measured in OIB (Fig. 6; Chaussidon and Marty, 1995; Tanaka and  
330 Nakamura, 2005; Genske et al., 2014; Brounce et al., 2012), but are notably much more  
331 tightly defined. These  $\delta^{11}\text{B}$  values are consistently lighter than those found in arcs, like  
332 Kamchatka (Ishikawa et al., 2001; De Hoog and Savov, 2018), and overlap with values  
333 from arcs where younger, hotter, oceanic crust is being subducted, like the Cascades  
334 (Leeman et al., 2004; Savov et al., 2009; Walowski et al., 2016).

335

## 336 **5. Discussion**

### 337 **5.1 Crustal assimilation and seawater alteration**

338 Due to the relatively high B abundance and elevated  $\delta^{11}\text{B}$  values in seawater (4.5  
339  $\mu\text{g/g}$ , +39.5‰; Spivak and Edmond, 1987; Foster et al., 2010), minor assimilation (<3%)  
340 of seawater, brines, or seawater-altered materials can significantly increase the B contents  
341 and the  $\delta^{11}\text{B}$  of the otherwise low-boron basaltic melt (Ryan et al., 1996; Marschall et al.,  
342 2017). Thus, identifying the possible influence of assimilation is essential for determining  
343 the correct composition of the mantle source region for OIB.

344 Our primary use of melt inclusions decreases the potential for assimilation of  
345 seawater-altered materials. The melt inclusions should be armored against contamination

post-entrapment and so it is useful to estimate the depth at which this occurs. It is well-established that the ratio of H<sub>2</sub>O/CO<sub>2</sub> dissolved in silicate melts is sensitive to pressure (e.g., Newman and Lowenstern, 2002). Despite uncertainty that melt inclusions preserve the initial volatile concentrations due to post-entrapment processes such as CO<sub>2</sub>-loss to vapor bubbles (e.g., Wallace et al., 2015) and H-diffusion (Bucholz et al., 2013; Gaetani et al., 2012; Walowski et al., 2015), the dissolved H<sub>2</sub>O/CO<sub>2</sub> should nonetheless provide minimum estimates of entrapment depths. For example, Figure 3b shows that the Piton de Caille melt inclusions were trapped at or deeper than ~7.5 km (assuming an average crustal density of 3.0 g/cm<sup>3</sup>). These minimum depth estimates are within the lower crust (crustal thickness beneath La Réunion is ~12 km; Fontaine et al., 2015) and confirms that the analyzed melt inclusions had far less opportunity for interaction with crustal materials than submarine glasses, decreasing the opportunity of seawater contamination and assimilation of altered oceanic crust (AOC).

At La Palma, melt inclusions from each locality sampled more variably degassed melts. Figure 3d shows that all melt inclusion suites, excluding BF02, contain melt inclusions trapped at or greater than ~10.5 km (assuming an average crustal density of 3.0 g/cm<sup>3</sup>). With MOHO depths beneath La Palma estimated at ~12 km (Fullea et al., 2015), these depths of entrapment are within the lower crust, although other mineralogical evidence suggests crystallization of primitive magmas may begin sub-MOHO (Klügel et al., 2005; Nikogosian et al., 2002). This indicates that the least degassed melt inclusions from La Palma had little interaction with crustal materials. It is perhaps not surprising that the least degassed samples from BF01 display the most primitive compositions and are hosted in the highest forsterite olivine measured in this study. Thus, this sample likely

provides the most robust estimate of  $\delta^{11}\text{B}$  for the HIMU-like mantle source beneath La Palma.

In addition to focusing on un-degassed melt inclusions, Figure 4 shows variability of  $\delta^{11}\text{B}$  with independent metrics that may indicate assimilation of hydrothermally altered lithologies. For example, if  $\delta^{11}\text{B}$  was influenced by assimilation during crustal transit and magmatic evolution, positive correlations would be expected between  $\delta^{11}\text{B}$  and B concentrations, while negative correlations would be expected between  $\delta^{11}\text{B}$  and host olivine Fo%. Furthermore, assessment of sea-water related contamination can be obtained from ratios of halogens to other incompatible elements, such as Cl/K (Stroncik and Haase, 2004; Kendrick et al., 2014) due to the high abundance of halogens in seawater. Previous work has shown the relationships between Cl/K versus K can be used to discriminate between seawater contamination, degassing and magmatic fractionation (Stroncik and Haase, 2004). For our samples, we find that each suite of melt inclusions shows no meaningful correlations between  $\delta^{11}\text{B}$  and B, Cl/K<sub>2</sub>O, or the composition (Fo%) of host olivine crystals that might hint at crustal contamination (Fig. 4). Rather, each suite shows variability only with respect to  $\delta^{11}\text{B}$  (y-axis; Fig. 4). This pattern indicates that for most samples, the range of  $\delta^{11}\text{B}$  within a given melt inclusion suite is related to analytical uncertainty of the  $\delta^{11}\text{B}$  measurement, and is not the result of a magmatic process.

Conversely, subaerial glasses from BF01 display elevated  $\delta^{11}\text{B}$  and B relative to BF01 MI, but have lower values of Cl/K<sub>2</sub>O as the result of degassing (Fig. 4a and b). Because Cl is degassed, it is not possible to use halogens to identify assimilation of seawater-altered material for this sample (BF01 glass). However, the statistically

significant change in  $\delta^{11}\text{B}$  between melt trapped at depth as inclusions and a more evolved melt erupted as glass at the surface suggests that minor contamination may have occurred during magmatic evolution after melt inclusion entrapment. Additionally, melt inclusions from BF02 also contain higher concentrations of B and isotopically heavier  $\delta^{11}\text{B}$  compared to BF01 melt inclusions, which are derived from a proximal locality. In addition to melt inclusions being degassed (Fig. 3d, Fig. 4b) and compositionally evolved (Fig. 4c), similar to the BF01 subaerial glass, this observation provides evidence that BF02 may have experienced minor amounts of B contamination, and thus, should not be used to determine mantle source  $\delta^{11}\text{B}$ . Therefore, we exclude BF02 and BF01 glass from the remainder of the discussion figures and analyses. As discussed above, all other samples from both La Palma and La Réunion show no systematic variation in B,  $\delta^{11}\text{B}$ , host-olivine Fo, or halogens, which highlights that undegassed melt inclusions retain  $\delta^{11}\text{B}$  values most representative of the mantle source region, and are not likely influenced by assimilation en route to the surface.

## **5.2 The $\delta^{11}\text{B}$ composition of the primitive mantle**

Due to the ability for boron isotopes to trace recycled materials in the deep mantle, a number of studies have used the boron isotopic system to characterize the OIB reservoirs that have been consistently recognized by Sr-Nd-Pb isotopes (Fig. 5; e.g., Chaussidon and Jambon, 1994; Chaussidon and Marty, 1995; Chaussidon and Marty 1995; Gurenko and Chaussidon 1997; Roy-Barman et al. 1998; Tanaka and Nakamura, 2005; Brounce et al., 2012; and Genske et al., 2014). A comprehensive attempt to characterize the  $\delta^{11}\text{B}$  composition of the ‘primitive mantle’ as sampled by OIB is

described in Chaussidon and Marty (1995). In this study, submarine glasses from Hawaii, St. Helena, Iceland, Macdonald Seamount, Afar, and the Galapagos were analyzed. The results found a large range in  $\delta^{11}\text{B}$  (-15 to +7‰), and thus, an “OIB source”  $\delta^{11}\text{B}$  had to be calculated based on the most primitive and highest  $^3\text{He}/^4\text{He}$  samples, and was determined to be  $-10\pm 2\text{‰}$  (Fig. 5). Subsequent work, however, produced contradictory results (e.g., Tanaka and Nakamura, 2005), interpreted their results on a MORB baseline that has since been redefined (Marschall et al., 2017), or most often, identified that samples were contaminated by hydrothermally or seawater altered materials en route to the surface (Fig. 5; Brounce et al., 2012; Gurenko et al., 2014). Thus, a robust value for the  $\delta^{11}\text{B}$  composition of the ‘primitive mantle’ or OIB-mantle-source has remained elusive.

Recent work by Marschall et al. (2017), however, does provide a well-constrained value for pristine, uncontaminated MORB (and the DMM) of  $-7.1\text{‰}\pm 0.9\text{‰}$ . The study, which investigated 56 MORBs from the Mid-Atlantic Ridge, the Southwest Indian Ridge, and the East Pacific Rise and carefully screened for contamination utilizing  $\text{Cl}/\text{K}$  (which was shown to elevate  $\delta^{11}\text{B}$  to values as high as  $-2.2\pm 1.7\text{‰}$ ), also found no difference between N-MORB and E-MORB reservoirs. Additional  $\delta^{11}\text{B}$  for samples from the South Atlantic were presented by Dixon et al. (2017), the compositions of which ( $\delta^{11}\text{B} = -7.7\pm 1.9\text{‰}$ ) were close to that of the Marschall et al. (2017) MORB datum. The samples were derived from the plume-influenced Discovery and Shona anomalies and are therefore not representative for uncontaminated MORB. However, depleted samples (i.e., closest to MORB compositions) averaged to lower  $\delta^{11}\text{B}$  than enriched samples ( $-9.2\pm 1.5\text{‰}$  vs  $-6.4\pm 1.1\text{‰}$ ), suggesting that perhaps the South Atlantic mantle might be



lighter than average MORB mantle. Further work will be needed to confirm this as the Dixon et al. (2017) samples were not as rigorously screened for the effects of shallow crustal processes as the Marschall et al. (2017) data, which may have contributed to the variability. This considered, because we use similar standard materials and reference values as Marschall et al., (2017) and described in Marschall and Monteleone (2015), we subsequently compare our results confidently to this MORB datum.

Several aspects of La Réunion magmas point to a source little disturbed by recent plate recycling (see section 2.1) and so our multiple, well-clustered  $\delta^{11}\text{B}$  analyses from La Réunion should provide a useful estimate for the deep, primitive mantle. Our mean  $\delta^{11}\text{B}$  for La Réunion ( $-7.9\pm0.5\text{‰}$ ) overlaps within uncertainty of the global MORB dataset ( $-7.1\pm0.9\text{‰}$ ), suggesting that the primitive mantle may be indistinguishable from MORB with respect to  $\delta^{11}\text{B}$ . Alternatively, because La Réunion is produced by relatively large degrees of melting relative to other OIB, indicated by tholeiitic compositions and trace element models (see Supplementary Fig. 2), this observation may be explained by boron acquired in the upper mantle. That is, a low-B concentration primitive mantle component may be diluted by MORB-source mantle B and  $\delta^{11}\text{B}$  during partial melting or re-equilibration in the uppermost mantle.

### **5.3 Boron in the mantle source**

To better constrain the boron isotope systematics at La Palma and La Réunion, it is necessary to understand the relative abundance of boron in the mantle source regions. The major element compositions of melt inclusions from La Palma, which are silica-undersaturated, and La Réunion, which extend to tholeiitic compositions, alone

emphasize the petrogenetic differences between these two suites. Therefore, to determine whether or not source variability exists with respect to B, it is useful to consider differences in the degree of partial melting of mantle source regions. Relationships between Zr/Y and La/Y (Supplementary Fig. 2) are used to quantify different degrees of melting and show that La Palma samples represent smaller degree partial melts (2-3%) compared with La Réunion samples (~10%), and affirm that all melts were predominantly generated in the garnet-facies mantle. Using a simple modal batch melting equation, the estimated melt percent, and a range in estimated bulk partition coefficients for B (using the analogs  $D_{Pr} = 0.026$  and  $D_{Ce} = 0.017$ ; Marschall et al., 2017), a mantle source B concentration can be calculated for each locality. To achieve the average B concentration measured in La Réunion melt inclusions (2.46  $\mu\text{g/g}$ ) in a 10% partial melt, the mantle source should contain ~0.31-0.28  $\mu\text{g/g}$  B. For the most primitive sample from La Palma, BF01, an average measured B concentration of 2.36  $\mu\text{g/g}$  is achieved from melting a mantle source with ~0.14-0.11  $\mu\text{g/g}$  by 3%. These results highlight that, despite similar averages in measured melt B concentrations, the mantle source beneath La Palma is estimated to contain less than half as much B as the mantle source beneath La Réunion, although both OIB source regions contain higher concentrations than estimates for the depleted-MORB-mantle (0.077  $\mu\text{g/g}$ ; Marschall et al., 2017).

Due to the inherent uncertainty with melting models, we can additionally explore source heterogeneity through comparison of trace element ratios (e.g., Jochum et al., 1989). During mantle melting, B exhibits similar incompatibility to light REE, such as Ce and La, and partitions similarly to Be, Pr, Pb, and Zr during basalt fractionation (Marschall et al., 2017). Thus, Figure 6 shows the covariance of B/Zr and B/Ce with

respect to  $\delta^{11}\text{B}$ . The distinctly lighter  $\delta^{11}\text{B}$  signatures of La Palma samples correlates with lower B/Zr and B/Ce than at La Réunion. This relationship, in conjunction with the calculated mantle source B concentrations, suggests that the mantle source reservoir for the La Palma HIMU-like magmas has lower concentrations of B than the primitive mantle reservoir sampled at La Réunion.

## **5.5 The $\delta^{11}\text{B}$ variability in OIB mantle sources**

As discussed in section 2.2, previous work has shown that the mantle source beneath La Palma has clear contributions from a recycled component (e.g., Day et al., 2010). Our new B isotopes results are consistent with these previous hypotheses in that La Palma samples show anomalously low  $\delta^{11}\text{B}$ , B/Zr, and B/Ce. Thus, the mantle source at La Palma requires a component with isotopically light B and low B abundance. Light boron isotope signatures can be generated at or near the surface and are typically found in material such as continental crust and siliceous oceanic sediments (e.g., Marschall, 2018; Trumbull and Slack, 2018). However, in addition to a light  $\delta^{11}\text{B}$  signature, the La Palma mantle source has B concentrations depleted relative to MORB that cannot be simply explained by the mixing of these B-enriched materials (i.e., sediment or continental crust) into the mantle, as this would create a source enriched in B relative to MORB or the primitive mantle. Nor are the radiogenic isotopic signatures consistent with the contribution of continental material. Therefore, a preferred explanation of a B-depleted and isotopically light mantle source is derived from subducted oceanic lithosphere that has been effectively stripped of B during subduction dehydration, consistent with

observations at arc volcanoes (e.g., Ryan et al., 1995; Walowski et al., 2016; De Hoog and Savov, 2018 and references there within).

To test this hypothesis, we model mixing a 3% partial melt of a hypothetical “dehydrated oceanic lithosphere” endmember with an upper mantle melt (Fig. 7; average MORB defined by Marschall et al., 2017). Due to uncertainty in the fractionation of  $\delta^{11}\text{B}$  during subduction dehydration, we utilize two different model endmembers to represent the recycled component. The first endmember, with a  $\delta^{11}\text{B}$  value of -35‰, is based on the oceanic lithosphere dehydration model of Marschall et al., (2007a), assuming a phengite-free eclogite lithology at 2.5 GPa. However, recent experimental constraints indicate the pH of supercritical fluids during subduction dehydration may be more alkaline than previously suggested (Galvez et al., 2017), and thus, in addition to uncertainty in fractionation factors, the fractionation of  $\delta^{11}\text{B}$  at depth may not be as significant as previously understood. Hence, we additionally model mixing using the  $\delta^{11}\text{B}$  model results of Konrad-Schmolke and Halama (2014). We find that mixing of a dehydrated slab endmember with  $\delta^{11}\text{B}$  values from -11 to -22‰ (correlated to depths of slab dehydration between ~140-200 km depth; Konrad-Schmolke and Halama, 2014) best-predicts the range in measured  $\delta^{11}\text{B}$  from the La Palma melt inclusion suites. The mixing model further indicates that the La Palma magmas have ~65-85% of their B contributed from the recycled component, although uncertainty of this simplified model can influence the exact mixing proportions with MORB. Additional uncertainty arises from the fact that the subduction dehydration model endmembers (i.e., Marschall et al., 2007a; Konrad-Schmolke and Halama, 2014) utilize modern seawater compositions ( $\delta^{11}\text{B} = +39.5\text{‰}$ ), although the hypothesized recycled component in the La Palma HIMU-

source is <1.8 Ga (Day et al., 2010). While the  $\delta^{11}\text{B}$  of Precambrian seawater is poorly constrained (Marschall et al., 2018), published estimates for Archean seawater (+14 $\pm$ 15‰ and +27 $\pm$ 11‰, Grew et al., 2015 and Chaussidon and Appel, 1997, respectively) are isotopically lighter than modern seawater, which would necessitate an even lighter model endmember. Despite these various uncertainties, the mixing model results importantly highlight that dehydrated recycled oceanic lithosphere retains enough B to leverage the  $\delta^{11}\text{B}$  composition and produce the B concentrations and isotopic values observed in the La Palma mantle source.

#### **5.4 The volatile composition of OIB mantle sources**

In addition to understanding how two different deep mantle sources compare in their  $\delta^{11}\text{B}$  systematics compared to MORB, a secondary goal of this study is to better understand the concentrations and distribution of volatiles in deep recycled mantle material. To this end, Figure 8a and 8b show the covariance of  $\text{H}_2\text{O}_{\text{max}}/\text{Ce}$  ( $\text{H}_2\text{O}_{\text{max}}$  referring to the maximum  $\text{H}_2\text{O}$  measured in each melt inclusion suite as a best estimate for initial  $\text{H}_2\text{O}$  content) with  $\delta^{11}\text{B}$  and  $^{206}\text{Pb}/^{204}\text{Pb}$ . Consistent with observations of B/Zr and the dehydrated oceanic lithosphere source hypothesis, La Palma samples have a lower  $\text{H}_2\text{O}_{\text{max}}/\text{Ce}$  than samples from La Réunion and MORB (Fig. 8a), producing positive correlations between  $\text{H}_2\text{O}_{\text{max}}/\text{Ce}$  and  $\delta^{11}\text{B}$ . During slab dehydration,  $\text{H}_2\text{O}$  is progressively stripped from the slab, while Ce is buffered in the presence of epidote (Carter et al., 2015), producing order of magnitude decreases in  $\text{H}_2\text{O}/\text{Ce}$  with increasing T and P (e.g., Cooper et al., 2012). Therefore, dehydrated oceanic lithosphere would be expected to have low  $\text{H}_2\text{O}_{\text{max}}/\text{Ce}$  ratios (i.e., BF01  $\text{H}_2\text{O}_{\text{max}}/\text{Ce}$  = 187). It is notable that the observed

H<sub>2</sub>O<sub>max</sub>/Ce is even more depleted than most MORB (H<sub>2</sub>O<sub>max</sub>/Ce = 150-400) and the primitive mantle (La Réunion H<sub>2</sub>O<sub>max</sub>/Ce = 252). Interestingly, this observation is consistent with previous studies on HIMU melts, which also find H<sub>2</sub>O<sub>max</sub>/Ce values lower than MORB. For example, the HIMU mantle source at Mangaia was determined by Cabral et al. (2014) using re-homogenized melt inclusions to have a H<sub>2</sub>O<sub>max</sub>/Ce ratio of ~200, while Dixon et al. (2002) calculated a H<sub>2</sub>O<sub>max</sub>/Ce ratio of ~100 for the HIMU source. Both Cabral et al. (2014) and Dixon et al. (2002) conclude that these low primary magmatic H<sub>2</sub>O<sub>max</sub>/Ce ratios are consistent with significant dehydration of oceanic crust of >80% efficiency during subduction, followed by long-term storage in the mantle. Similar to the mixing model described in Figure 7, we also model mixing between an upper mantle melt and the two potential HIMU endmembers determined by Dixon et al. (2002) and Cabral et al. (2014; Fig. 8a). Figure 8 shows that the La Palma melts are best explained by mixing of the lower H<sub>2</sub>O<sub>max</sub>/Ce HIMU source, as determined by Dixon et al., (2002), with either enriched or depleted upper mantle melts. Conversely, the Mangaia HIMU endmember has H<sub>2</sub>O<sub>max</sub>/Ce values that are too elevated to reproduce the measured values at La Palma. These results provide additional support that the HIMU source reservoir is likely depleted in both H<sub>2</sub>O and B due to efficient stripping of these light elements during subduction dehydration.

Despite the possibility of CO<sub>2</sub> post-entrapment loss to vapor bubbles for which we have not corrected, undegassed melt inclusions from La Palma retain some of the highest CO<sub>2</sub> contents directly measured in OIB (up to 4303 µg/g; e.g., Koleszar et al., 2009). These high CO<sub>2</sub> concentrations are similar to previous studies of HIMU melt inclusions (e.g., Cabral et al., 2014) and are consistent with the experimental studies that require a

carbonated protolith in the mantle source in order to generate highly alkaline rocks and small degree partial melts (e.g., Kiseeva et al., 2013). That considered,  $\text{CO}_{2\text{max}}/\text{Nb}$  ratios of La Palma melt inclusions (~40-60) are lower than those at La Réunion (~70-95), and both significantly lower than MORB (~530; Cartigny et al., 2008).

## 6. Conclusion

Although it has been well-established that recycling of the lithosphere via subduction drives the chemical evolution of the mantle, the character and distribution of volatiles in various mantle reservoirs remains uncertain. In this study, we provide new contributions that improve this understanding through a comparison of the volatile and  $\delta^{11}\text{B}$  compositions of olivine-hosted melt inclusions from contrasting OIB endmembers from La Palma, Canary Islands, and La Réunion Island. Our new dataset shows that tephra-derived olivine-hosted melt inclusions are protected from contamination during ascent and provide more robust estimates of primary  $\delta^{11}\text{B}$  than previous bulk rock studies, highlighting that the aforementioned OIB reservoirs have distinctly different  $\delta^{11}\text{B}$  compositions. That is, tholeiitic basalts from La Réunion Island have  $\delta^{11}\text{B}$  signatures ( $-7.9 \pm 0.5\text{‰}$ ) that overlap with the global MORB dataset ( $-7.1 \pm 0.9\text{‰}$ ), while HIMU-like alkali basalts from La Palma, Canary Islands display  $\delta^{11}\text{B}$  compositions which extend to lighter values ( $-10.5 \pm 0.7\text{‰}$ ). In concert with B/Zr and  $\text{H}_2\text{O}/\text{Ce}$ , these results provide evidence that the mantle source sampled at La Réunion, representative of a deeply sourced primitive mantle, is indistinguishable from MORB with respect to B and  $\text{H}_2\text{O}$ . Because the La Réunion source has been shown to have little to no influence from recycled components, we hypothesize that either the primitive mantle has an isotopic

fingerprint indistinguishable from MORB or that B concentrations are sufficiently low that they are diluted by partial melting that occurs in the uppermost mantle. Conversely, we find the HIMU-like mantle source beneath La Palma contains low-B and low-H<sub>2</sub>O, which is best explained by contributions from a recycled oceanic lithosphere component significantly dehydrated and isotopically fractionated within the ‘subduction factory,’ in the uppermost mantle. Our results provide new support for the role of complex and step-wise subduction zone processing in the generation of radiogenic Pb-isotopic signatures, and the decoupling volatiles and light stable isotopes from other lithophile elements in OIB mantle reservoirs.

## **Acknowledgements**

We thank J. Craven and R. Hinton for assistance with the SIMS measurements, C. Hayward for assistance with the EPMA, and B. Upton for providing the Piton de Caille samples. We also thank H. Marschall and J. Ryan for their insightful reviews and M. Bickle for editorial handling. Constructive discussions facilitated by NERC Deep Volatiles Consortium meetings are gratefully acknowledged. Funding was provided by National Environmental Research Council grant NE/M000443/1.

## **Table Captions**

*Table 1:* Average melt inclusion compositions. Average compositions refer to the average MI composition calculated from the full suite of analyzed melt inclusions (n = X refers to number of melt inclusions from each sample). Major element uncertainty calculated as one standard deviation of the population used to calculate the average from MI suite



(including analytical uncertainty). The complete corrected and uncorrected dataset of individual MI compositions can be found in Supplementary Tables TS2 and TS3.

<sup>a</sup>Initial Fe contents used in the calculations were chosen based either on the  $\text{FeO}^T$  of the bulk tephra or the highest value of  $\text{FeO}^T$  for MI from a particular cone.

<sup>b</sup> $\text{H}_2\text{O}_{\text{max}}$  values represent the highest from each cone after post-entrapment crystallization correction

<sup>c</sup> $\text{CO}_{2\text{max}}$  values represent the highest from each cone after post-entrapment crystallization correction

<sup>d</sup>Refers to the average percent olivine addition required to reach equilibrium with host olivine compositions

## Figure Captions

*Figure 1: Sample Localities.* (a) Topographic shade map showing the relative location of sampled ocean islands; the Canary Island Archipelago is off the northwestern coast of the African continent and the island of La Réunion is off the eastern coast of Madagascar. (b) Topographic shade map depicting the island of La Réunion and highlighting the location of the Piton de Caille, the cinder cone sampled for this study. (c) Regional map of the Canary Island chain showing the location of La Palma relative to the other islands of the archipelago. La Palma and El Hierro represent the youngest islands in a generally westward-younging chain. (d) Topographic shade map of La Palma showing individual sample localities, Barranco de Fagundo, a Holocene Cone, and Vólcan Duraznero, which erupted in 1949. Basemaps generated with GeoMapApp (<http://www.geomapapp.org>; Ryan et al., 2009).

644

645 *Figure 2:* The  $^{87}\text{Sr}/^{86}\text{Sr}$  and  $^{206}\text{Pb}/^{204}\text{Pb}$  of OIB globally. Individual colored data points as  
646 described in the legend represent previously published bulk rock values from the sample  
647 localities used in this study (B. Fagundo, Holocene Cone, and Vólcan Duraznero, from  
648 Day et al., 2010; and La Réunion: Albarède et al., 1997 and references there within). The  
649 larger maroon shaded region outlines previously published data from La Réunion Island  
650 and Piton de la Fournaise volcano (Albarède et al., 1997 and references there within) and  
651 the teal shaded region represents all previously published data from other samples from  
652 the Cumbre Vieja Rift Zone and the Taburiente Shield at La Palma (Praegel et al., 2006;  
653 Day et al., 2010). The grey shaded regions represent previously published datasets from  
654 notable ocean island endmembers (data from the GEOROC Database [http://georoc.mpch-](http://georoc.mpch-mainz.gwdg.de/georoc/)  
655 [mainz.gwdg.de/georoc/](http://georoc.mpch-mainz.gwdg.de/georoc/) and references there within). Colors and symbols for La Palma  
656 and Réunion samples as described in the legend are consistent throughout the following  
657 figures.

658

659 *Figure 3:* Melt inclusion major element and volatile compositions compared to  
660 previously published melt inclusion and bulk rock data. All melt inclusions from La  
661 Palma and La Réunion plotted in this figure are corrected for post-entrapment  
662 crystallization as described in Section 5.3 (Supplementary Table TS2 and TS3). (a,c)  
663 MgO versus  $\text{Al}_2\text{O}_3$  contents of melt inclusions from (a) Piton Caille compared to  
664 previously published data from La Réunion Island, including melt inclusion data from  
665 Piton Caille (Bureau et al., 1998), proximal Holocene cinder cones (Dolomieu and Piton  
666 Vincenzo; Bureau et al., 1998), and Piton de la Fournaise (Vigouroux et al., 2009), and

whole rock data from Piton de La Fournaise (Albarède et al., 1997). (c) La Palma melt inclusion data compared to previously published whole rock data from both the Cumbre Vieja Rift and Taburiente Shield (Day et al., 2010). The overlapping red bars indicate an approximation for the most primitive compositions from each island, and red arrows show the influence of olivine and pyroxene fractionation of accumulation from that parental melt composition. (b, d) H<sub>2</sub>O versus CO<sub>2</sub> contents of (b) La Réunion and (d) La Palma melt inclusions with vapor saturation isobars generated using Sol\_Ex (grey lines; Witham et al., 2012) and open-system degassing paths (black lines) from Newman and Lowenstern (2002). The Sol\_Ex input composition (open star symbol) is based on major element data the most primitive and un-degassed melt inclusion from each individual sample. We interpret nearly vertical trends in H<sub>2</sub>O versus CO<sub>2</sub> as CO<sub>2</sub> degassing prior to entrapment, while variability in H<sub>2</sub>O away from open system degassing paths is likely the result of post-entrapment diffusive H<sub>2</sub>O-loss.

*Figure 4:* The  $\delta^{11}\text{B}$  composition of individual melt inclusions versus (a) B ( $\mu\text{g/g}$ ), (b) Cl/K<sub>2</sub>O, and (c) the forsterite percent of host olivine crystals. The B, Cl, and K<sub>2</sub>O concentrations from all MI plotted in this figure are corrected for post-entrapment crystallization as described in Section 5.3 (Supplementary Table TS2 and TS3). Each panel is used as a different method to test whether  $\delta^{11}\text{B}$  is changing as a function of magmatic evolution driven by assimilation of B-enriched material (i.e., seawater or seawater altered materials) or fractional crystallization. Each sample suite of melt inclusions show no meaningful positive or negative correlations between  $\delta^{11}\text{B}$  and (a) B ( $\mu\text{g/g}$ ), (b) Cl/K<sub>2</sub>O, or (c) the forsterite percent of host olivine crystals. Rather, each suite

shows variability only with respect to  $\delta^{11}\text{B}$  (y-axis). This pattern indicates that for most samples, the range of  $\delta^{11}\text{B}$  represents the analytical uncertainty, and is not the result of a magmatic process. That being said, B. Fagundo 02 has heavier  $\delta^{11}\text{B}$  values with elevated B ( $\mu\text{g/g}$ ) concentrations and hosts MI in lower forsterite olivine crystals when compared to melt inclusions from a similar location, B. Fagundo 01. Although these samples are different, their proximal location and geochemical relationship suggests that B. Fagundo 02 melt inclusions may have altered  $\delta^{11}\text{B}$  values and do not provide robust estimates of the mantle source  $\delta^{11}\text{B}$ , as indicated by the red arrow labeled “assimilation”. Thus, B. Fagundo 01, are utilized exclusively in the following figures as the most robust estimate of primary  $\delta^{11}\text{B}$  for the B. Fagundo locality at La Palma.

*Figure 5:* The average  $\delta^{11}\text{B}$  composition of samples from this study compared to a selection of previously published OIB samples. The filled colored symbols represent the average  $\delta^{11}\text{B}$  of each melt inclusion suite (# of inclusions for each sample as in *Table 1*) from La Palma and La Réunion, with error bars/symbol size representing  $2\sigma$  uncertainty. The grey bar represents MORB with  $2\sigma$  uncertainty (Marschall et al., 2017). Black symbols represent individual analyses of submarine glassed from Hawaii, the Galapagos, the Azores, and St. Helena (Chaussidon and Marty, 1995). The black rectangle labeled “OIB” is a calculated “OIB source” composition as described in Chaussidon and Marty (1995), with a  $2\sigma$  uncertainty. Grey diamonds represent analyses of individual melt inclusions from Lakagígar, Iceland, with the largest symbol representing the best estimate of the initial  $\delta^{11}\text{B}$  (Brounce et al., 2012). Grey triangles represent analyses of individual melt inclusions from the Azores (Flores and Corvo), with the largest symbol representing

the best estimate of the initial  $\delta^{11}\text{B}$  (Genske et al., 2014). Grey crosses represent lavas from Hawaii (Koolau, Kilauea, and Mauna Loa; Tanaka and Nakamura, 2005). For a detailed overview of all currently published OIB B-isotope data, see Marschall, 2018.

*Figure 6:*  $\delta^{11}\text{B}$  versus B/Zr for MI suite averages with error bars that represent  $2\sigma$  uncertainty, and the individual MI compositions from which the averages are calculated. The B and Zr concentrations from all MI data plotted in this figure are corrected for post-entrapment crystallization as described in Section 5.3 (Supplementary Table TS2 and TS3). Because B has is similarly incompatible to Zr (Marschall et al., 2017), ratios of these elements can be used to assess relative mantle source B abundances, despite difference in degree of mantle melting or minor amounts of crystal fractionation. The black diamond represents the average MORB composition as defined by Marschall et al. (2017).

*Figure 7:*  $\delta^{11}\text{B}$  versus B/Zr for MI suite averages with error bars that represent  $2\sigma$  uncertainty, data as described in Fig. 6. Plotted curves represent mixing between a 3% partial melt of a hypothetical recycled mantle component (black and grey hexagons; dehydrated oceanic lithosphere) with average MORB (Marschall et al., 2017; black oval). The  $\delta^{11}\text{B}$  value for the isotopically light recycled endmember (grey hexagon) is based on the model results of Marschall et al. (2007a), while the  $\delta^{11}\text{B}$  for the heavier recycled component (black hexagon) is based on the range in model results from Konrad-Schmolke and Halama (2014; black hexagon) that best-predict the measured  $\delta^{11}\text{B}$

compositions. The Zr composition is derived from a refractory eclogite composition (Rudnick et al., 2002 and references there within).

*Figure 8:  $H_2O_{max}/Ce$  versus (a)  $\delta^{11}B$  versus and (b)  $^{206}Pb/^{204}Pb$ . Colored symbols for MI suite averages from this study as described in legend with  $2\sigma$  error bars. Plotted curves on panel (a) represent mixing between a 3% partial melt of previously determined HIMU mantle reservoirs (black stars; Mangaia HIMU from Cabral et al., 2014; ‘HIMU source’ from Dixon et al., 2002) with both S. Mid-Atlantic Ridge MORB (grey hexagon) and Arctic Ridge MORB (black hexagon; Dixon et al., 2017). Panel (b) shows a comparison of previously published submarine MORB glass data (Dixon et al., 2017) and OIB data (Tanaka et al., 2002, Hémond et al., 1994, Workman et al., 2004, Snyder et al., 2004 and references there within). The  $\delta^{11}B$  is based on the range in model results (-17 to -11‰; from Konrad-Schmolke and Halama, 2014) that best-predict the measured  $\delta^{11}B$  compositions.*

## References

- Allègre, C. J. (1982). Chemical geodynamics. *Tectonophysics*, 81(3-4), 109-132.
- Albarède, F., Luais, B., Fitton, G., Semet, M., Kaminski, E., Upton, B. G. J., & Cheminée, J. L. (1997). The geochemical regimes of Piton de la Fournaise volcano (Réunion) during the last 530,000 years. *Journal of Petrology*, 38(2), 171-201.

757 Borisov, A. A., & Shapkin, A. I. (1990). A new empirical equation rating Fe<sup>3+</sup>/Fe<sup>2+</sup> in  
 758 magmas to their composition, oxygen fugacity, and temperature. *Geochem. Int.*, 27(1),  
 759 111-116.  
 760  
 761 Brounce, M., Feineman, M., LaFemina, P., & Gurenko, A. (2012). Insights into crustal  
 762 assimilation by Icelandic basalts from boron isotopes in melt inclusions from the 1783–  
 763 1784 Lakagigar eruption. *Geochimica et Cosmochimica Acta*, 94, 164-180.  
 764  
 765 Brounce M., Stolper E., Peterson M., & Eiler J. (2017). Goldschmidt Abstracts, 2017,  
 766 475.  
 767  
 768 Bucholz, C. E., Gaetani, G. A., Behn, M. D., & Shimizu, N. (2013). Post-entrapment  
 769 modification of volatiles and oxygen fugacity in olivine-hosted melt inclusions. *Earth  
 770 and Planetary Science Letters*, 374, 145-155.  
 771  
 772 Bureau, H., Pineau, F., Métrich, N., Semet, M. P., & Javoy, M. (1998). A melt and fluid  
 773 inclusion study of the gas phase at Piton de la Fournaise volcano (Réunion  
 774 Island). *Chemical geology*, 147(1-2), 115-130.  
 775  
 776  
 777 Cabral, R. A., Jackson, M. G., Koga, K. T., Rose-Koga, E. F., Hauri, E. H., Whitehouse,  
 778 M. J., ... & Kelley, K. A. (2014). Volatile cycling of H<sub>2</sub>O, CO<sub>2</sub>, F, and Cl in the HIMU

779 mantle: A new window provided by melt inclusions from oceanic hot spot lavas at  
780 Mangaia, Cook Islands. *Geochemistry, Geophysics, Geosystems*, 15(11), 4445-4467.  
781

782 Carter, L. B., Skora, S., Blundy, J. D., De Hoog, J. C. M., & Elliott, T. (2015). An  
783 experimental study of trace element fluxes from subducted oceanic crust. *Journal of*  
784 *Petrology*, 56(8), 1585-1606.  
785

786 Cartigny, P., Pineau, F., Aubaud, C., & Javoy, M. (2008). Towards a consistent mantle  
787 carbon flux estimate: Insights from volatile systematics (H<sub>2</sub>O/Ce, δD, CO<sub>2</sub>/Nb) in the  
788 North Atlantic mantle (14 N and 34 N). *Earth and Planetary Science Letters*, 265(3-4),  
789 672-685.  
790

791 Chase, C. G. (1981). Oceanic island Pb: two-stage histories and mantle evolution. *Earth*  
792 *and Planetary Science Letters*, 52(2), 277-284.  
793

794 Chaussidon, M., & Jambon, A. (1994). Boron content and isotopic composition of  
795 oceanic basalts: geochemical and cosmochemical implications. *Earth and Planetary*  
796 *Science Letters*, 121(3-4), 277-291.  
797

798 Chaussidon, M., & Marty, B. (1995). Primitive boron isotope composition of the  
799 mantle. *Science*, 269(5222), 383-386.  
800



801 Chaussidon, M., & Appel, P. W. U. (1997). Boron isotopic composition of tourmalines  
802 from the 3.8-Ga-old Isua supracrustals, West Greenland: implications on the  $\delta^{11}\text{B}$  value  
803 of early Archean seawater. *Chemical Geology*, 136(3-4), 171-180.

804

805 Chauvel, C., Hofmann, A. W., & Vidal, P. (1992). HIMU-EM: the French Polynesian  
806 connection. *Earth and Planetary Science Letters*, 110(1-4), 99-119.

807

808 Cooper, L. B., Ruscitto, D. M., Plank, T., Wallace, P. J., Syracuse, E. M., & Manning, C.  
809 E. (2012). Global variations in H<sub>2</sub>O/Ce: 1. Slab surface temperatures beneath volcanic  
810 arcs. *Geochemistry, Geophysics, Geosystems*, 13(3).

811

812 Danyushevsky, L. V., Della-Pasqua, F. N., & Sokolov, S. (2000). Re-equilibration of  
813 melt inclusions trapped by magnesian olivine phenocrysts from subduction-related  
814 magmas: petrological implications. *Contributions to Mineralogy and Petrology*, 138(1),  
815 68-83.

816

817 Danyushevsky, L. V., & Plechov, P. (2011). Petrolog3: Integrated software for modeling  
818 crystallization processes. *Geochemistry, Geophysics, Geosystems*, 12(7).

819

820 Day, J. M., Pearson, D. G., Macpherson, C. G., Lowry, D., & Carracedo, J. C. (2010).  
821 Evidence for distinct proportions of subducted oceanic crust and lithosphere in HIMU-  
822 type mantle beneath El Hierro and La Palma, Canary Islands. *Geochimica et*  
823 *Cosmochimica Acta*, 74(22), 6565-6589.

824

825 De Hoog, C. J., & Savov, I. P. (2017). Subduction zones, dehydration, metasomatism,  
826 mud and serpentinite volcanoes, and arc magmatism. *Boron isotopes—The fifth element,*  
827 *advances in isotope geochemistry*, 7, 219-249.

828

829 Dixon, J. E., Leist, L., Langmuir, C., & Schilling, J. G. (2002). Recycled dehydrated  
830 lithosphere observed in plume-influenced mid-ocean-ridge basalt. *Nature*, 420(6914),  
831 385.

832

833 Dixon, J. E., Bindeman, I. N., Kingsley, R. H., Simons, K. K., Le Roux, P. J., Hajewski,  
834 T. R., Walowski, K.J., Wada, I. & Wallace, P.J. (2017). Light Stable Isotopic  
835 Compositions of Enriched Mantle Sources: Resolving the Dehydration  
836 Paradox. *Geochemistry, Geophysics, Geosystems*, 18(11), 3801-3839.

837

838 Eiler, J. M., Farley, K. A., Valley, J. W., Hauri, E., Craig, H., Hart, S. R., & Stolper, E.  
839 M. (1997). Oxygen isotope variations in ocean island basalt phenocrysts. *Geochimica et*  
840 *Cosmochimica Acta*, 61(11), 2281-2293.

841

842 Esposito, R., Steele-Macinnis, M. J., Fedele, L., & Bodnar, R. J. (2010, June). Evolution  
843 of H<sub>2</sub>O and CO<sub>2</sub> contents in silicate melt inclusions during post-entrapment  
844 crystallization. *Geochimica et Cosmochimica Acta*, 74(12), A272-A272.

845

846 Fontaine, F. R., Barruol, G., Tkalčić, H., Wölbern, I., Rümpker, G., Bodin, T., &  
847 Haugmard, M. (2015). Crustal and uppermost mantle structure variation beneath La  
848 Réunion hotspot track. *Geophysical Journal International*, 203(1), 107-126.

849

850 Foster, G. L., Pogge von Strandmann, P. A., & Rae, J. W. B. (2010). Boron and  
851 magnesium isotopic composition of seawater. *Geochemistry, Geophysics, Geosystems*,  
852 11(8).

853

854 Fulla, J., Camacho, A. G., Negredo, A. M., & Fernández, J. (2015). The Canary Islands  
855 hot spot: new insights from 3D coupled geophysical–petrological modelling of the  
856 lithosphere and uppermost mantle. *Earth and Planetary Science Letters*, 409, 71-88.

857

858 Gaetani, G. A., O’Leary, J. A., Shimizu, N., Bucholz, C. E., & Newville, M. (2012).  
859 Rapid reequilibration of H<sub>2</sub>O and oxygen fugacity in olivine-hosted melt  
860 inclusions. *Geology*, 40(10), 915-918.

861

862 Galvez, M. E., Connolly, J. A., & Manning, C. E. (2016). Implications for metal and  
863 volatile cycles from the pH of subduction zone fluids. *Nature*, 539(7629), 420.

864

865 Genske, F. S., Turner, S. P., Beier, C., Chu, M. F., Tonarini, S., Pearson, N. J., & Haase,  
866 K. M. (2014). Lithium and boron isotope systematics in lavas from the Azores islands  
867 reveal crustal assimilation. *Chemical Geology*, 373, 27-36.

868

869 Grew, E. S., Dymek, R. F., De Hoog, J. C., Harley, S. L., Boak, J., Hazen, R. M., &  
870 Yates, M. G. (2015). Boron isotopes in tourmaline from the ca. 3.7–3.8 Ga Isua  
871 supracrustal belt, Greenland: Sources for boron in Eoarchean continental crust and  
872 seawater. *Geochimica et Cosmochimica Acta*, 163, 156-177.

873

874 Gurenko, A. A., & Chaussidon, M. (1997). Boron concentrations and isotopic  
875 composition of the Icelandic mantle: evidence from glass inclusions in olivine. *Chemical*  
876 *Geology*, 135(1), 21-34.

877

878 Gurenko, A. A., & Kamenetsky, V. S. (2011). Boron isotopic composition of olivine-  
879 hosted melt inclusions from Gorgona komatiites, Colombia: New evidence supporting  
880 wet komatiite origin. *Earth and Planetary Science Letters*, 312(1-2), 201-212.

881

882 Harvey, J., Garrido, C. J., Savov, I., Agostini, S., Padrón-Navarta, J. A., Marchesi, C., &  
883 Gómez-Pugnaire, M. T. (2014). <sup>11</sup>B-rich fluids in subduction zones: The role of antigorite  
884 dehydration in subducting slabs and boron isotope heterogeneity in the mantle. *Chemical*  
885 *Geology*, 376, 20-30.

886

887 Harvey, J., Savov, I. P., Agostini, S., Cliff, R., Walshaw, R., 2014, Si-metasomatism in  
888 serpentized peridotite: the effects of talc-alteration on strontium and boron isotopes in  
889 abyssal peridotites from ODP Leg 209, Hole 1268a. *Geochim. Cosmochim. Acta*, 126, 30-  
890 48.

891

892 Hémond, C., Devey, C. W., & Chauvel, C. (1994). Source compositions and melting  
 893 processes in the Society and Austral plumes (South Pacific Ocean): Element and isotope  
 894 (Sr, Nd, Pb, Th) geochemistry. *Chemical Geology*, 115(1-2), 7-45.  
 895  
 896 Hernández-Pacheco, E., & Valls, M. C. (1982). *The historic eruptions of La Palma island*  
 897 *(Canaries)*.  
 898  
 899 Hofmann, A. W., & White, W. M. (1982). Mantle plumes from ancient oceanic  
 900 crust. *Earth and Planetary Science Letters*, 57(2), 421-436.  
 901  
 902 Ishikawa, T., & Nakamura, E. (1993). Boron isotope systematics of marine  
 903 sediments. *Earth and Planetary Science Letters*, 117(3-4), 567-580.  
 904  
 905 Ishikawa, T., & Tera, F. (1999). Two isotopically distinct fluid components involved in  
 906 the Mariana arc: Evidence from Nb/B ratios and B, Sr, Nd, and Pb isotope  
 907 systematics. *Geology*, 27(1), 83-86.  
 908  
 909 Ishikawa, T., Tera, F., & Nakazawa, T. (2001). Boron isotope and trace element  
 910 systematics of the three volcanic zones in the Kamchatka arc. *Geochimica et*  
 911 *Cosmochimica Acta*, 65(24), 4523-4537  
 912  
 913 Johnson, E. R., Wallace, P. J., Delgado Granados, H., Manea, V. C., Kent, A. J.,  
 914 Bindeman, I. N., & Donegan, C. S. (2009). Subduction-related volatile recycling and

915 magma generation beneath Central Mexico: insights from melt inclusions, oxygen  
 916 isotopes and geodynamic models. *Journal of Petrology*, 50(9), 1729-1764.  
 917

918 Jung, H., & Karato, S. I. (2001). Water-induced fabric transitions in olivine.  
 919 *Science*, 293(5534), 1460-1463.  
 920

921 Kendrick, M. A., Kamenetsky, V. S., Phillips, D., & Honda, M. (2012). Halogen  
 922 systematics (Cl, Br, I) in mid-ocean ridge basalts: a Macquarie Island case  
 923 study. *Geochimica et Cosmochimica Acta*, 81, 82-93.  
 924

925 Kendrick, M. A., Jackson, M. G., Kent, A. J., Hauri, E. H., Wallace, P. J., & Woodhead,  
 926 J. (2014). Contrasting behaviours of CO<sub>2</sub>, S, H<sub>2</sub>O and halogens (F, Cl, Br, and I) in  
 927 enriched-mantle melts from Pitcairn and Society seamounts. *Chemical Geology*, 370, 69-  
 928 81.  
 929

930 Kiseeva, E. S., Litasov, K. D., Yaxley, G. M., Ohtani, E., & Kamenetsky, V. S. (2013).  
 931 Melting and phase relations of carbonated eclogite at 9–21 GPa and the petrogenesis of  
 932 alkali-rich melts in the deep mantle. *Journal of Petrology*, 54(8), 1555-1583.  
 933

934 Koleszar, A. M., Saal, A. E., Hauri, E. H., Nagle, A. N., Liang, Y., & Kurz, M. D.  
 935 (2009). The volatile contents of the Galapagos plume; evidence for H<sub>2</sub>O and F open  
 936 system behavior in melt inclusions. *Earth and Planetary Science Letters*, 287(3), 442-  
 937 452.

938

939 Kowalski, P., & Wunder, B. (2017). Boron-isotope fractionation among solids-fluids-  
940 melts: experiments and atomic modeling. *Boron isotopes—The fifth element, advances in*  
941 *isotope geochemistry*, 7, 33-69.

942

943 Klügel, A., Hansteen, T. H., & Galipp, K. (2005). Magma storage and underplating  
944 beneath Cumbre Vieja volcano, la Palma (Canary Islands). *Earth and Planetary Science*  
945 *Letters*, 236(1), 211-226.

946

947 Konrad-Schmolke, M., & Halama, R. (2014). Combined thermodynamic–geochemical  
948 modeling in metamorphic geology: boron as tracer of fluid–rock interaction. *Lithos*, 208,  
949 393-414.

950

951 Leeman, W. P., Tonarini, S., Chan, L. H., & Borg, L. E. (2004). Boron and lithium  
952 isotopic variations in a hot subduction zone—the southern Washington  
953 Cascades. *Chemical Geology*, 212(1), 101-124.

954

955 Lloyd, A. S., Plank, T., Ruprecht, P., Hauri, E. H., & Rose, W. (2013). Volatile loss from  
956 melt inclusions in pyroclasts of differing sizes. *Contributions to Mineralogy and*  
957 *Petrology*, 165(1), 129-153.

958

959 Marcantonio, F., Zindler, A., Elliott, T., & Staudigel, H. (1996). Os isotope systematics  
 960 of La Palma, Canary Islands: evidence for recycled crust in the mantle source of HIMU  
 961 ocean islands. *Oceanographic Literature Review*, 2(43), 153.

962

963 Marschall, H. R., & Monteleone, B. D. (2015). Boron isotope analysis of silicate glass  
 964 with very low boron concentrations by secondary ion mass spectrometry. *Geostandards*  
 965 *and Geoanalytical Research*, 39(1), 31-46.

966

967 Marschall, H. R., Wanless, V. D., Shimizu, N., von Strandmann, P. A. P., Elliott, T., &  
 968 Monteleone, B. D. (2017). The boron and lithium isotopic composition of mid-ocean  
 969 ridge basalts and the mantle. *Geochimica et Cosmochimica Acta*, 207, 102-138.

970

971 Marschall, H. R. (2018) Boron isotopes in the ocean floor realm and the mantle. In:  
 972 Marschall, H. R. & Foster, G. L. (eds.) *Boron Isotopes – The Fifth Element*, vol. 6 of  
 973 *Advances in Isotope Geochemistry*, chap. 8, 189–215, Springer, Heidelberg

974

975 McBirney, A. R., & Gass, I. G. (1967). Relations of oceanic volcanic rocks to mid-  
 976 oceanic rises and heat flow. *Earth and Planetary Science Letters*, 2(4), 265-276.

977

978 Michael, P. (1995). Regionally distinctive sources of depleted MORB: Evidence from  
 979 trace elements and H<sub>2</sub>O. *Earth and Planetary Science Letters*, 131(3-4), 301-320.

980



981 Nielsen, S. G., Rehkämper, M., Norman, M. D., Halliday, A. N., & Harrison, D. (2006).  
 982 Thallium isotopic evidence for ferromanganese sediments in the mantle source of  
 983 Hawaiian basalts. *Nature*, 439(7074), 314.  
 984  
 985 Moore, L. R., Gazel, E., Tuohy, R., Lloyd, A. S., Esposito, R., Steele-MacInnis, M., &  
 986 Bodnar, R. J. (2015). Bubbles matter: An assessment of the contribution of vapor bubbles  
 987 to melt inclusion volatile budgets. *American Mineralogist*, 100(4), 806-823.  
 988  
 989 Nakamura, E., Ishikawa, T., Birck, J. L., & Allègre, C. J. (1992). Precise boron isotopic  
 990 analysis of natural rock samples using a boron-mannitol complex. *Chemical*  
 991 *Geology*, 94(3), 193-204.  
 992  
 993 Newman, S., & Lowenstern, J. B. (2002). VolatileCalc: a silicate melt–H<sub>2</sub>O–CO<sub>2</sub>  
 994 solution model written in Visual Basic for excel. *Computers & Geosciences*, 28(5), 597-  
 995 604.  
 996  
 997 Nikogosian, I. K., Elliott, T., & Touret, J. L. (2002). Melt evolution beneath thick  
 998 lithosphere: a magmatic inclusion study of La Palma, Canary Islands. *Chemical*  
 999 *Geology*, 183(1), 169-193.  
 1000  
 1001 Pabst, S., Zack, T., Savov, I. P., Ludwig, T., Rost, D., Tonarini, S., & Vicenzi, E. P.  
 1002 (2012). The fate of subducted oceanic slabs in the shallow mantle: insights from boron

1003 isotopes and light element composition of metasomatized blueschists from the Mariana  
 1004 forearc. *Lithos*, 132, 162-179.  
 1005  
 1006 Peters, B. J., Carlson, R. W., Day, J. M., & Horan, M. F. (2018). Hadean silicate  
 1007 differentiation preserved by anomalous  $^{142}\text{Nd}/^{144}\text{Nd}$  ratios in the Réunion hotspot  
 1008 source. *Nature*, 555(7694), 89.  
 1009  
 1010 Praegel, N.O., Holm, P.M., (2006). Lithospheric contributions to the high-MgO basanites  
 1011 from the Cumbre Vieja Volcano, La Palma, Canary Islands and evidence for temporal  
 1012 variation in plume influence. *Journal of Volcanology and Geothermal Research*,  
 1013 149(2006), 213-239.  
 1014  
 1015 Putirka, K. D. (2005). Mantle potential temperatures at Hawaii, Iceland, and the mid-  
 1016 ocean ridge system, as inferred from olivine phenocrysts: Evidence for thermally driven  
 1017 mantle plumes. *Geochemistry, Geophysics, Geosystems*, 6(5).  
 1018  
 1019 Rosner, M., Rhede, D., & Erzinger, J. (2004). Heavy boron isotope compositions of back-  
 1020 arc lavas from the southern Lau-basin (Valu Fa Ridge). *Geochimica et Cosmochimica*  
 1021 *Acta*, 68, (11A599-A599).  
 1022  
 1023 Rosner, M., Wiedenbeck, M., & Ludwig, T. (2008). Composition-induced variations in  
 1024 SIMS instrumental mass fractionation during boron isotope ratio measurements of silicate  
 1025 glasses. *Geostandards and Geoanalytical Research*, 32(1), 27-38.

1026

1027 Rosner, M., & Meixner, A. (2004). Boron isotopic composition and concentration of ten  
1028 geological reference materials. *Geostandards and Geoanalytical Research*, 28(3), 431-  
1029 441.

1030

1031 Ryan, J. G., & Langmuir, C. H. (1993). The systematics of boron abundances in young  
1032 volcanic rocks. *Geochimica et Cosmochimica Acta*, 57(7), 1489-1498.

1033

1034 Ryan, J. G., Leeman, W. P., Morris, J. D., & Langmuir, C. H. (1996). The boron  
1035 systematics of intraplate lavas: Implications for crust and mantle evolution. *Geochimica*  
1036 *et Cosmochimica Acta*, 60(3), 415-422.

1037

1038 Ryan, J. G., & Kyle, P. R. (2004). Lithium abundance and lithium isotope variations in  
1039 mantle sources: insights from intraplate volcanic rocks from Ross Island and Marie Byrd  
1040 Land (Antarctica) and other oceanic islands. *Chemical Geology*, 212(1), 125-142.

1041

1042 Ryan, W.B.F., S.M. Carbotte, J.O. Coplan, S. O'Hara, A. Melkonian, R. Arko, R.A.  
1043 Weissel, V. Ferrini, A. Goodwillie, F. Nitsche, J. Bonczkowski, and R. Zemsky (2009),  
1044 Global Multi-Resolution Topography synthesis, *Geochem. Geophys. Geosyst.*, 10,  
1045 Q03014, doi:10.1029/2008GC002332.

1046

1047 Roy-Barman, M., Wasserburg, G. J., Papanastassiou, D. A., & Chaussidon, M. (1998).  
 1048 Osmium isotopic compositions and Re–Os concentrations in sulfide globules from  
 1049 basaltic glasses. *Earth and Planetary Science Letters*, 154(1), 331-347.  
 1050  
 1051 Savov, I. P., Leeman, W. P., Lee, C. T. A., & Shirey, S. B. (2009). Boron isotopic  
 1052 variations in NW USA rhyolites: Yellowstone, Snake River Plain, Eastern  
 1053 Oregon. *Journal of Volcanology and Geothermal Research*, 188(1), 162-172.  
 1054  
 1055 Schiano, P., David, K., Vlastélic, I., Gannoun, A., Klein, M., Nauret, F., & Bonnand, P.  
 1056 (2012). Osmium isotope systematics of historical lavas from Piton de la Fournaise  
 1057 (Réunion Island, Indian Ocean). *Contributions to Mineralogy and Petrology*, 164(5),  
 1058 805-820.  
 1059  
 1060 Schmincke, H. U. (1982). Volcanic and chemical evolution of the Canary Islands.  
 1061 In *Geology of the Northwest African continental margin* (pp. 273-306). Springer, Berlin,  
 1062 Heidelberg.  
 1063  
 1064 Smith, H. J., Spivack, A. J., Staudigel, H., & Hart, S. R. (1995). The boron isotopic  
 1065 composition of altered oceanic crust. *Chemical Geology*, 126(2), 119-135.  
 1066  
 1067 Snyder, D. C., Widom, E., Pietruszka, A. J., & Carlson, R. W. (2004). The role of open-  
 1068 system processes in the development of silicic magma chambers: a chemical and isotopic

1069 investigation of the Fogo A trachyte deposit, São Miguel, Azores. *Journal of*  
 1070 *Petrology*, 45(4), 723-738.  
 1071  
 1072 Sobolev, A. V., & Nikogosian, I. K. (1994). Petrology of long-lived mantle plume  
 1073 magmatism: Hawaii, Pacific and Reunion Island, *Indian Ocean. Petrology*, 2(2), 111-  
 1074 144.  
 1075  
 1076 Spivack, A. J., & Edmond, J. M. (1987). Boron isotope exchange between seawater and  
 1077 the oceanic crust. *Geochimica et Cosmochimica Acta*, 51(5), 1033-1043.  
 1078  
 1079 Stroncik, N. A., & Haase, K. M. (2004). Chlorine in oceanic intraplate basalts:  
 1080 Constraints on mantle sources and recycling processes. *Geology*, 32(11), 945-948.  
 1081 Tanaka, R., & Nakamura, E. (2005). Boron isotopic constraints on the source of  
 1082 Hawaiian shield lavas. *Geochimica et Cosmochimica Acta*, 69(13), 3385-3399.  
 1083  
 1084 Tanaka, R., Nakamura, E., & Takahashi, E. (2002). Geochemical evolution of Koolau  
 1085 volcano, Hawaii. *Hawaiian Volcanoes: Deep Underwater Perspectives*, 311-332.  
 1086  
 1087 Teng, F. Z., Li, W. Y., Ke, S., Marty, B., Dauphas, N., Huang, S., ... & Pourmand, A.  
 1088 (2010). Magnesium isotopic composition of the Earth and chondrites. *Geochimica et*  
 1089 *Cosmochimica Acta*, 74(14), 4150-4166.  
 1090

1091 Tonarini, S., Leeman, W. P., & Leat, P. T. (2011). Subduction erosion of forearc mantle  
 1092 wedge implicated in the genesis of the South Sandwich Island (SSI) arc: evidence from  
 1093 boron isotope systematics. *Earth and Planetary Science Letters*, 301(1), 275-284.  
 1094  
 1095 Trumbull, R. B., & Slack, J. F. (2018). Boron isotopes in the continental crust: granites,  
 1096 pegmatites, felsic volcanic rocks, and related ore deposits. In *Boron Isotopes* (pp. 249-  
 1097 272). Springer, Cham.  
 1098  
 1099 Turner, S., Hawkesworth, C., Rogers, N., & King, P. (1997). U/Th isotope disequilibria  
 1100 and ocean island basalt generation in the Azores. *Chemical Geology*, 139(1), 145-164.  
 1101  
 1102 Vigouroux, N., Williams-Jones, A. E., Wallace, P., & Staudacher, T. (2009). The  
 1103 November 2002 eruption of Piton de la Fournaise, Réunion: tracking the pre-eruptive  
 1104 thermal evolution of magma using melt inclusions. *Bulletin of volcanology*, 71(9), 1077.  
 1105  
 1106 Wallace, P. J., Kamenetsky, V. S., & Cervantes, P. (2015). Melt inclusion CO<sub>2</sub> contents,  
 1107 pressures of olivine crystallization, and the problem of shrinkage bubbles. *American*  
 1108 *Mineralogist*, 100(4), 787-794.  
 1109  
 1110 Walowski, K. J., Wallace, P. J., Hauri, E. H., Wada, I., & Clynne, M. A. (2015). Slab  
 1111 melting beneath the Cascade Arc driven by dehydration of altered oceanic  
 1112 peridotite. *Nature Geoscience*, 8(5), 404.

1113 Walowski, K. J., Wallace, P. J., Clynnne, M. A., Rasmussen, D. J., & Weis, D. (2016).  
 1114 Slab melting and magma formation beneath the southern Cascade arc. *Earth and*  
 1115 *Planetary Science Letters*, 446, 100-112.  
 1116  
 1117 Williams, H. M., & Bizimis, M. (2014). Iron isotope tracing of mantle heterogeneity  
 1118 within the source regions of oceanic basalts. *Earth and Planetary Science Letters*, 404,  
 1119 396-407.  
 1120  
 1121 Workman, R. K., Hart, S. R., Jackson, M., Regelous, M., Farley, K. A., Blusztajn, J., &  
 1122 Staudigel, H. (2004). Recycled metasomatized lithosphere as the origin of the Enriched  
 1123 Mantle II (EM2) end-member: Evidence from the Samoan Volcanic  
 1124 Chain. *Geochemistry, Geophysics, Geosystems*, 5(4).  
 1125  
 1126 Witham, F., Blundy, J., Kohn, S. C., Lesne, P., Dixon, J., Churakov, S. V., &  
 1127 Botcharnikov, R. (2012). SolEx: A model for mixed COHSCI-volatile solubilities and  
 1128 exsolved gas compositions in basalt. *Computers & Geosciences*, 45, 87-97.  
 1129  
 1130 Zindler, A., & Hart, S. (1986). Chemical geodynamics. *Annual review of earth and*  
 1131 *planetary sciences*, 14(1), 493-571.  
 1132  
 1133  
 1134  
 1135

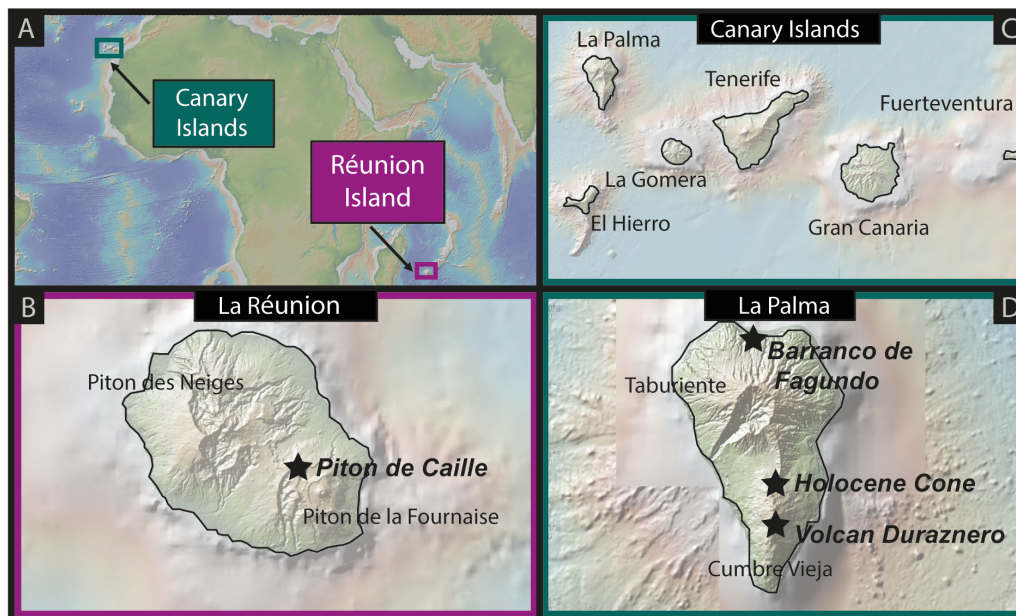


Figure 1



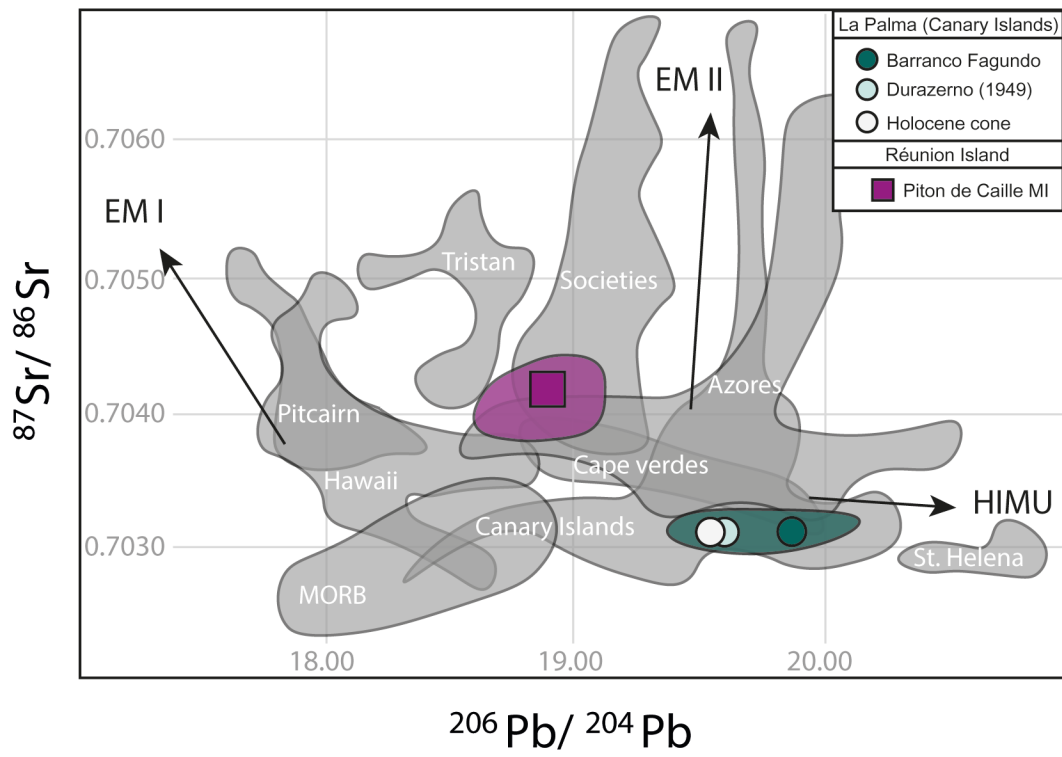


Figure 2

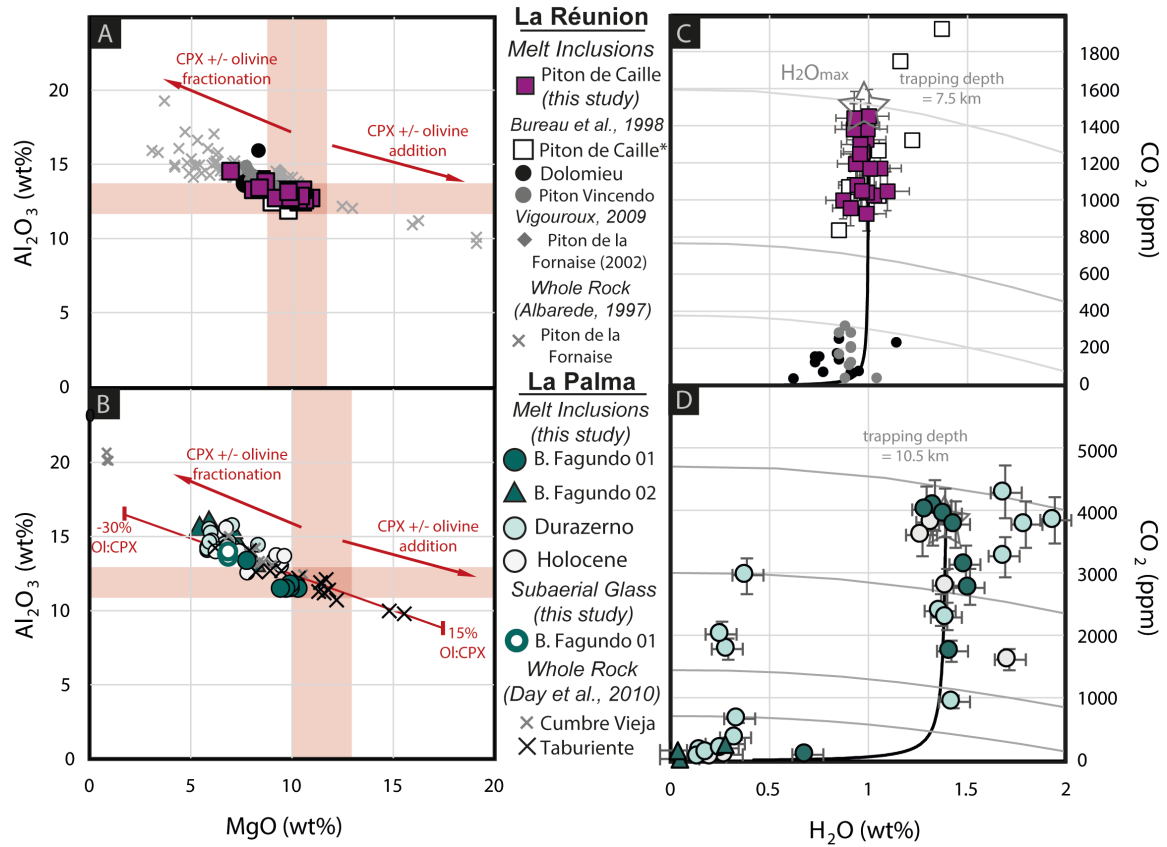


Figure 3

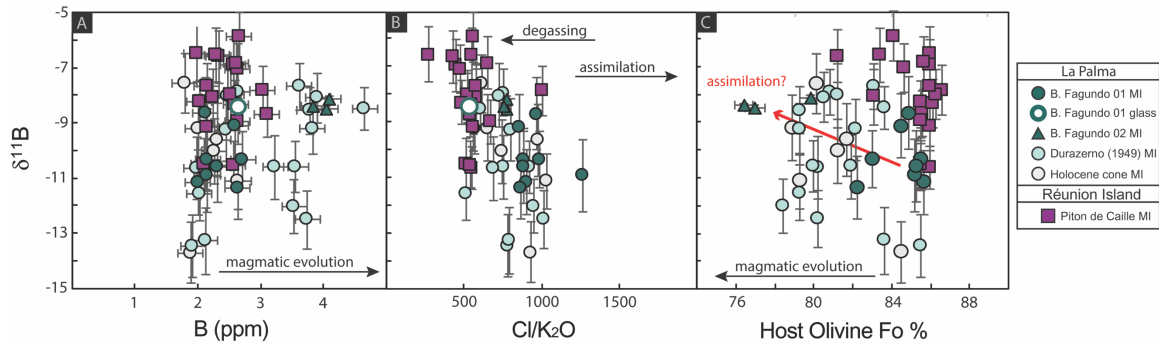


Figure 4

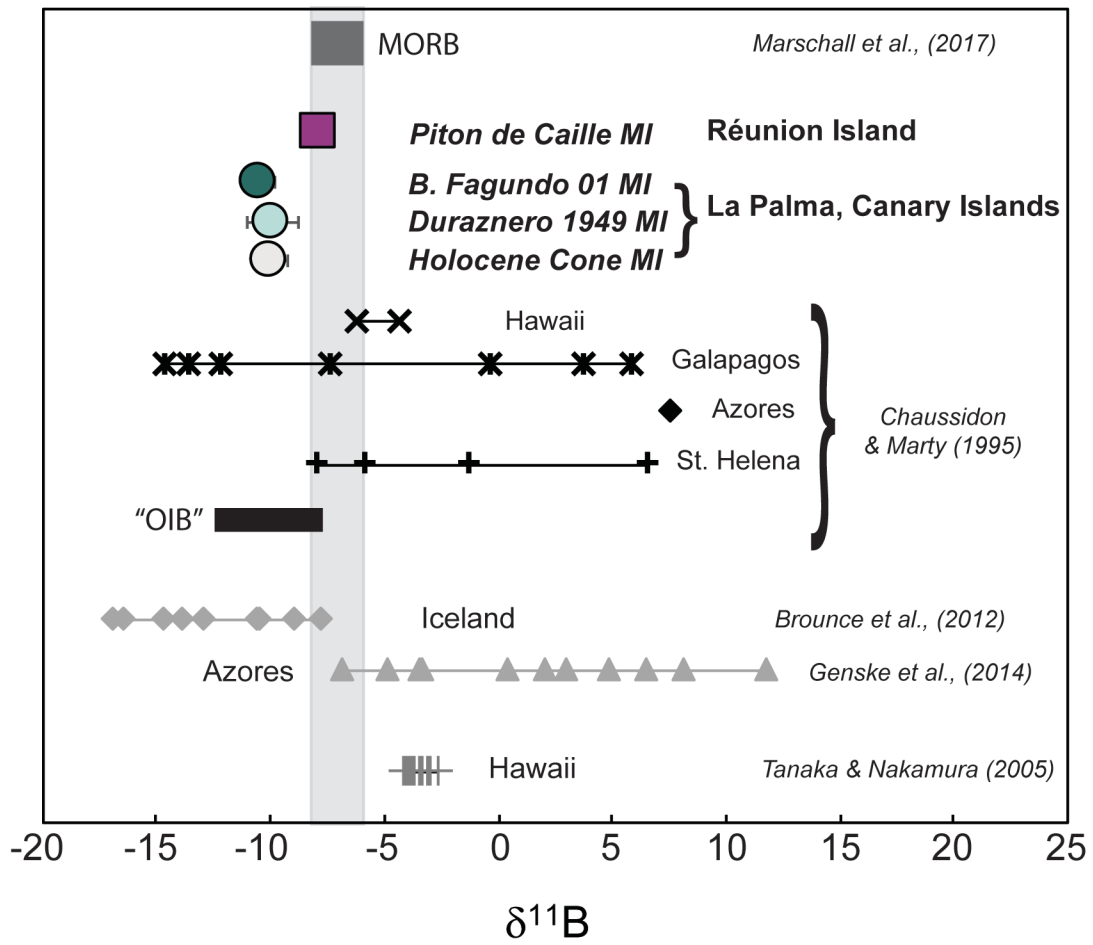


Figure 5

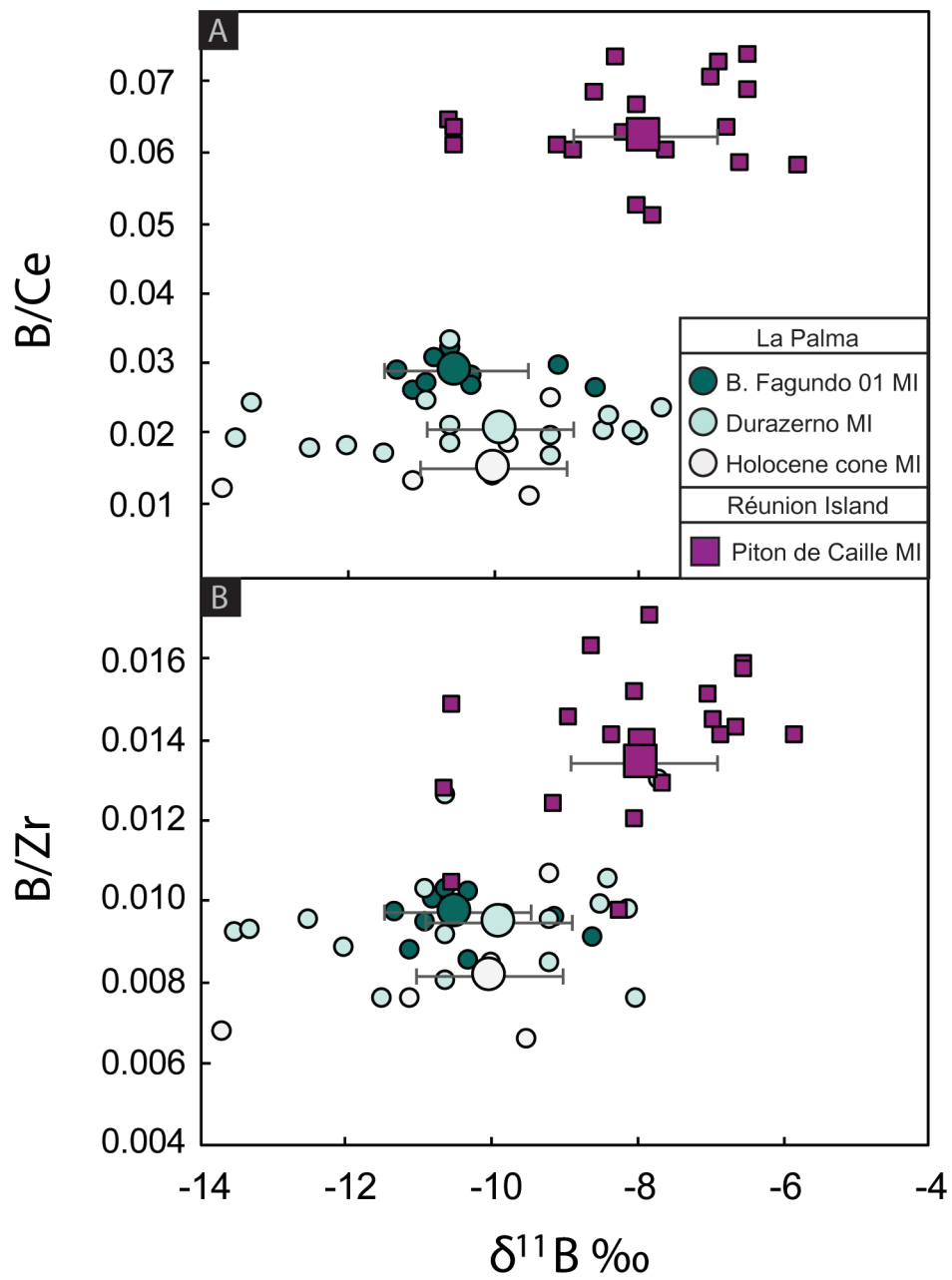


Figure 6

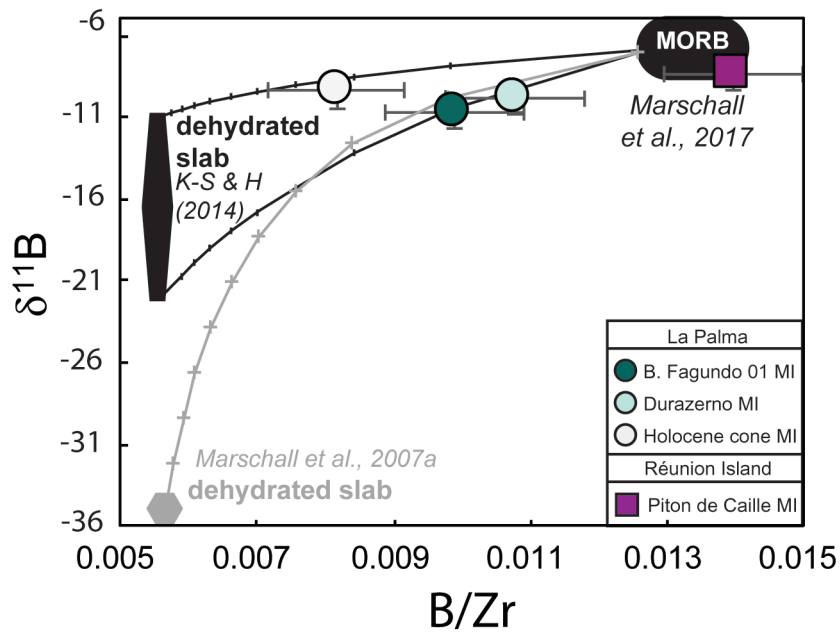


Figure 7

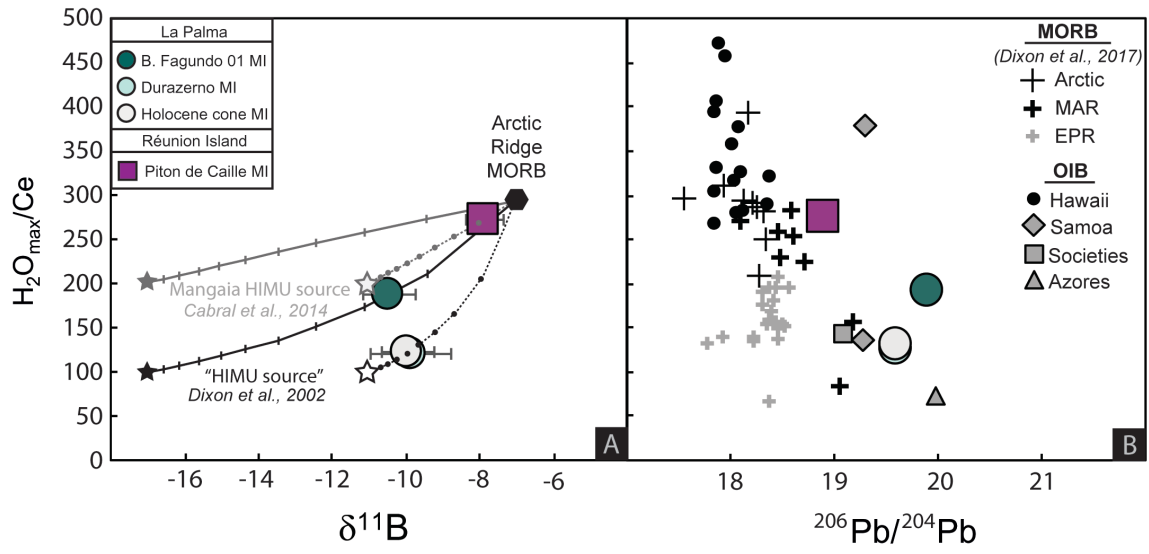


Figure 8